Single atom is not alone: Metal–support interactions in single-atom catalysis

Kun Qi, Manish Chhowalla, Damien Voiry

▶ **To cite this version:**

Kun Qi, Manish Chhowalla, Damien Voiry. Single atom is not alone: Metal–support interactions in single-atom catalysis. Materials Today, 2020, 40, pp.173-192. 10.1016/j.mattod.2020.07.002 . hal-03082865

HAL Id: hal-03082865
https://hal.science/hal-03082865

Submitted on 5 Oct 2021

HAL is a multi-disciplinary open access archive for the deposit and dissemination of scientific research documents, whether they are published or not. The documents may come from teaching and research institutions in France or abroad, or from public or private research centers.

L'archive ouverte pluridisciplinaire **HAL**, est destinée au dépôt et à la diffusion de documents scientifiques de niveau recherche, publiés ou non, émanant des établissements d'enseignement et de recherche français ou étrangers, des laboratoires publics ou privés.

Single Atom Is Not Alone: Metal-Support Interactions in Single-Atom Catalysis

Kun Qi[1], Manish Chhowalla[2], Damien Voiry[1*]

[1]*Institut Européen des Membranes, IEM, UMR 5635, Université Montpellier, ENSCM, CNRS, Montpellier, France*

[2]*Department of Materials Science and Metallurgy, University of Cambridge, Cambridge, UK*

Email: damien.voiry@umontpellier.fr

Abstract

Single-atom catalysts (SACs) have recently attracted interest in the fields of heterogeneous catalysis and electrocatalysis due to the enhancement in intrinsic activity and selectivity through optimized exposure of the active sites. Synthesis of SACs and research into their behavior have helped to elucidate the kinetics and thermodynamics of several key catalytic reactions. However, understanding the interactions between the metal single-atom active sites and the support matrix represents a notable challenge facing the development of atomically dispersed catalysts. Such interactions are essential in optimizing the reaction kinetics and maximizing the catalytic performance. This review explores the current state of the art in single-atom catalysis and critically analyzes the current understanding of metal-support interactions. Finally, we discuss the current challenges and future opportunities for development in the field.

Graphical Abstract

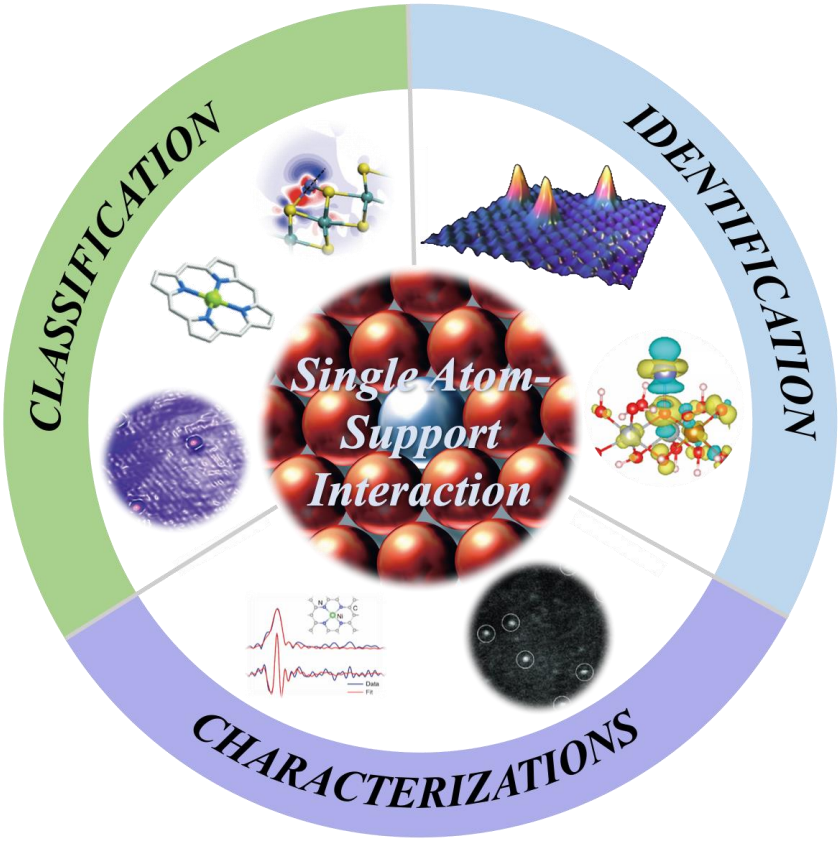

Introduction

Atomically dispersed catalysts with single metal atoms or mononuclear metal complexes anchored on supports represent the ideal platform for catalysis in terms of activity and efficient materials utilization.[1] However, considering that isolated metal atoms must be dispersed onto a substrate, a crucial parameter that determines the performance of SACs is the complex relationship between the coordination environment of the support and the metal atoms.[2] The lack of understanding regarding the interactions between the metal single atoms and the supports has hampered progress in improving the catalytic efficiency of the SACs.[3] The concept of strong metal-support interactions (MSI) and their importance in catalysis was first introduced by Tauster et al. in 1978 by showing that the hydrogen and carbon monoxide sorption capacity of noble metals supported on TiO_2 was affected by the nature of the interface between metal species and support.[4] SMSI helps stabilize the metal on the support and change the *d*-band center of the metal site, which can also perturb the local electronic structure of the support.[5, 6] The modification of the chemical state of metals caused by charge transfer at the interface plays a critical role in activating the reactants and affects the catalytic performance.[7] The understanding of MSI is still in its infancy because of difficulty in deconvolving its effects from intrinsic reaction parameters based on the properties of metal nanoparticle catalysts.[8] However, single-atom catalysts (SACs) provide an ideal platform to study metal-support interactions.[9] The strength of the interactions between single metal atoms and the supports is essential for the stabilization and activation of SACs.[10] Although strong interactions prevent metal atom aggregation, excessively strong interactions can render the atoms catalytically inactive.[11] In this paper, we review recent progress in understanding the interactions between single metal atoms and the supports. We summarize

the design and preparation of highly stable SACs and their catalytic activity. Then, we present recent advances in characterization techniques to identify the atomic and electronic structures of active sites at the metal support interface. Finally, the current challenges and future opportunities in the development of this field are discussed.

Single-atom-support interactions

Effective strategies to realize SACs are the starting point to study their catalytic mechanisms and origin of activity. The main challenge in preparing SACs is that their high surface energy enables them to agglomerate easily. Therefore, achieving stable SACs has become an important challenge in the field.[12] The key principle in preparation of SACs is tuning the single atom and support interaction such that they are sufficiently strong to prevent agglomeration but sufficiently weak to avoid significantly perturbing the electronic structure of the atom and keep it catalytically active.[13] The most common strategies to achieve SACs are to create anchor sites on the support *via* introduction of an electronic/structure disorder.[14] The nature of the support determines the coordination number, chemical bonding and steric environment that determine the geometric and electronic structures of the SACs.[15, 16] The interactions also affect the stability of SACs. Various types of supports have been explored: metals, various types of carbons and metal (hydr)oxides / nitrides / carbides / sulfides.

Metal supports

Single metal atoms (M1) anchored on a metal support (M2), which are referred to as single-atom alloys (SAAs), are thermodynamically more stable than other single-atom-support interactions. The atomically dispersed highly active sites in these SAAs can easily activate bonds to enable the uptake of species onto the surface and the subsequent spillover of adsorbed species onto the host metal, where

selective catalysis can be performed.[17, 18] For example, SAAs have been shown to activate C-H bonds at low temperatures without coke formation and selectively hydrogenate unsaturated hydrocarbons with excellent activity. As shown in **Figure 1**, the reported SAAs include Pt-Cu, Pt-$Al_{13}Fe_4$, Pd-Cu, Pd-Au, and Pd-Ag.[19-21] The two key factors to realize SAAs are the bonding energy and the concentration of single atoms. The bonding energy of M_1-M_2 should be stronger than M_1-M_1 to prevent the spontaneous nucleation of M_1.[22] M_1 should also be present in lower concentrations than M_2 to ensure that M_1 atoms are stabilized by bonding to the surrounding M_2 atoms to avoid aggregation. Other parameters such as the presence of grain boundaries or step edges have been found to stabilize individual atoms (**Figure 1c**).[23] Compared to other types of SACs, SAAs are more robust due to the formation of strong metal-metal bonds. In addition, the coordination and electronic properties can be finely tuned by varying the metal supports. This results in variable binding energies between the reagents, the intermediate species and the active sites which will orient the reaction in specific pathways .[24, 25]

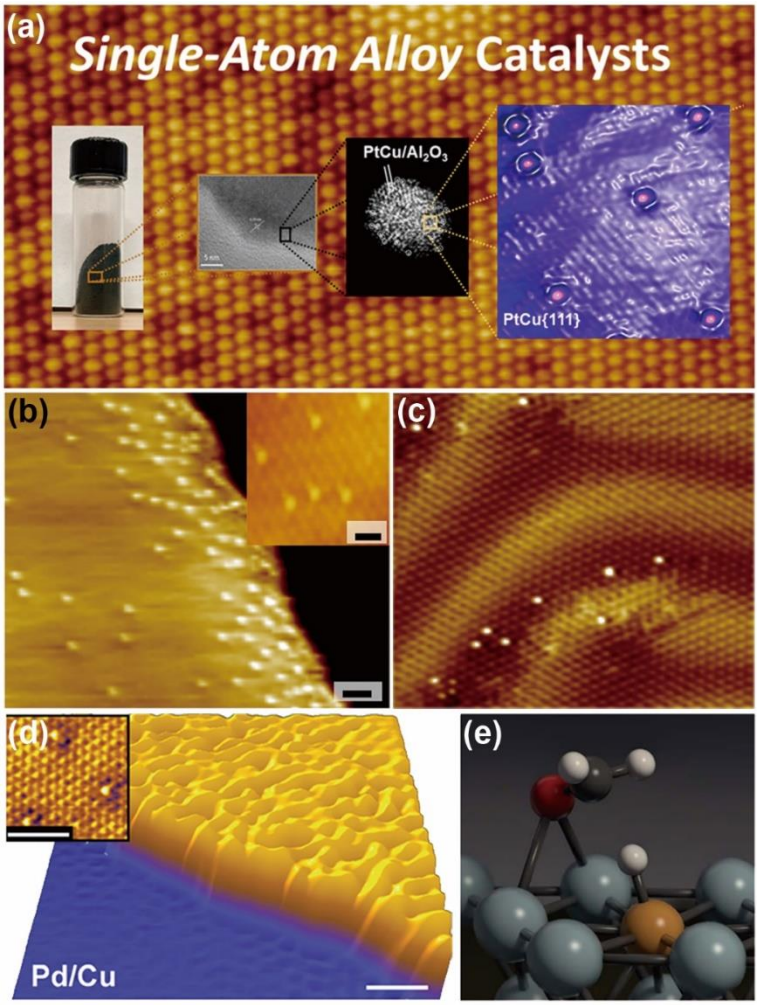

Figure 1 | Metal as supports for SACs. (a) STM image of 0.02 ML Pt/Cu(111) SAA surface, where the Pt atoms appear as isolated protrusions substituted into the Cu(111) surface. Reproduced from Ref. [18] with permission from Nature Publishing Group. (b) Wide-scale image of the Pt/Cu(111) SAA surface showing that Pt is distributed across both terraces and near the step edges. Reproduced from Ref. [19] with permission from Nature Publishing Group. (c) STM image of PdAu(111) SAA collected with -300 mV bias and 900 pA current. Reproduced from Ref. [23] with permission from the American Chemical Society. (d) Pd alloys into the Cu(111) surface preferentially above the step edges as evidenced by the rumpled appearance of the upper terrace. (Inset) Atomic resolution of the Pd/Cu alloy on the upper terrace showing individual, isolated Pd atoms in the surface layer, which appear as protrusions. Reproduced from Ref. [24] with permission from AAAS. (e) Calculated structures of the transition states of the rate-limiting step for methanol reforming on Cu, which provides insight to why AgCu exhibits a smaller activation energy. The single bond to H on AgCu is much stronger than that on bulk Cu. Cu, orange; Ag, gray; C, black; O, red; H, white. Reproduced from Ref. [25] with permission from Nature Publishing Group.

Carbon-based material supports

Carbon-based nanomaterials, especially graphene, graphdiyne and heteroatom (N, O, S and P)-doped sp2 carbon materials, have been extensively employed as supports for SACs.[26-28] Low-dimension sp2 carbons have important advantages, such as high surface area, high electronic conductivity and strong thermal stability.[29] Building well-defined molecular single-atom catalytic centers and linking them to a conductive carbon support are also preferred for bonding (**Figure 2a**).[30] For carbon-based nanomaterials, the single metal atoms can anchor at the edges (**Figure 2b**).[31] The presence of heteroatoms such as N, O and S stabilizes single metal atoms by forming stable metal-C, O, N and S σ-bonds, while metal-π interactions in carbon-based nanomaterials play an important role in stabilizing carbon-based nanomaterials.[27, 32] The strong electronic coupling between single metal atoms and carbon-based nanomaterials enables efficient charge transport between the catalytic active sites and the support, which enhances the catalytic property (**Figures 2c-2e**).[33-36]

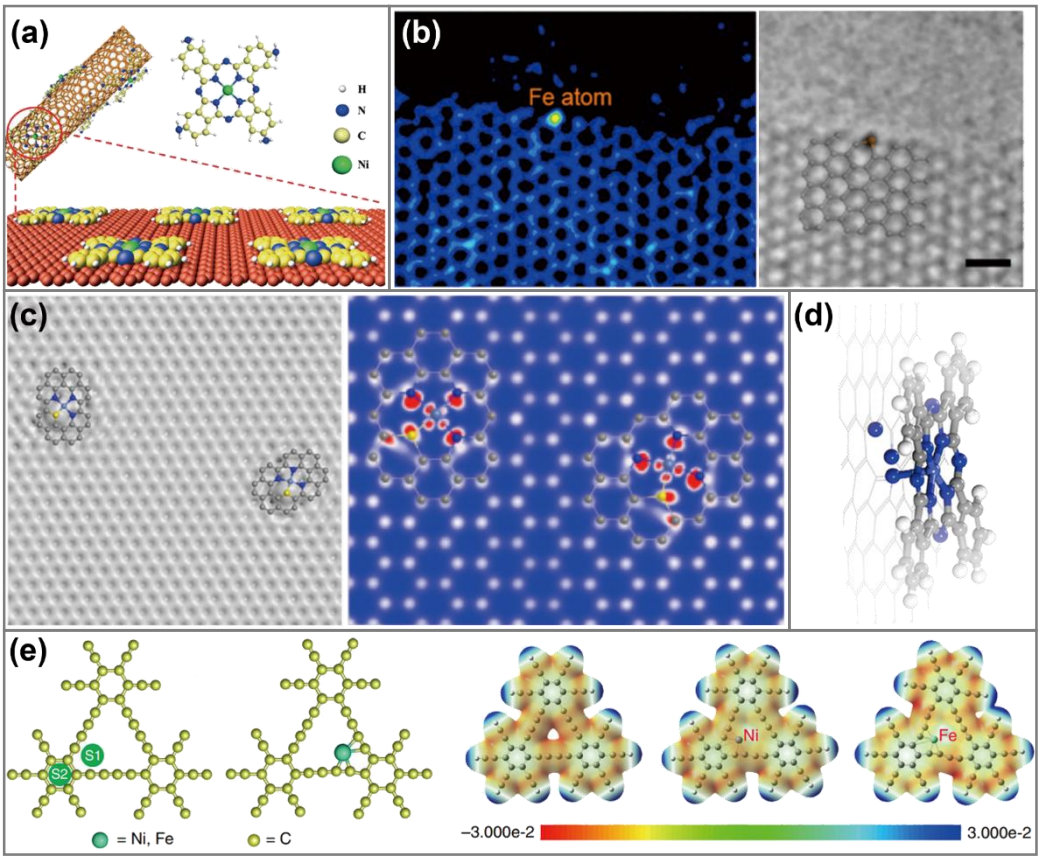

Figure 2 | Carbon-based materials as supports for SACs. (a) Synthesis schematic of model Ni SACs. Reproduced from Ref. [30] with permission from Wiley. (b) HRTEM images; magnified regions of HRTEM with overlaps of the DFT-calculated atomic structure of a distorted hexagon carbon including an Fe atom on the edge site. Reproduced from Ref. [31] with permission from Nature Publishing Group. (c) Simulated HRTEM and STM images for atomically disperse nickel-nitrogen-sulfur species embedded in porous carbon nanosheets. Reproduced from Ref. [33] with permission from Nature Publishing Group. (d) Schematic model for the single-atom Co-N_5 catalytic site, Co (wathet), N (blue), C (gray) and H (white). Reproduced from Ref. [34] with permission from the American Chemical Society. (e) Adsorption of single metal atoms on graphdiyne (GD) and optimized configuration electrostatic potential maps of pristine GD, Ni/GD, and Fe/GD. Reproduced from Ref. [35] with permission from Nature Publishing Group.

Metal (hydr)oxide / nitride / carbide / sulfide supports

Metal (hydr)oxides are the most used supports for heterogeneous catalysts because of their various geometric configurations, crystal phases, surface OH groups and anionic or cationic vacancies that serve as anchor sites for metal nanoparticles.[37] Thanks to their high specific surface areas, their

abundant metal or non-metal vacancies and their surface functional groups, metal (hydr)oxide / nitride / carbide / sulfide present many advantages compared to other supports in stabilizing single metal atoms.[3] In particular, the (hydr)oxides of reducible metal ions such as W^{6+} and Fe^{3+} are widely used to stabilize single metal atoms by bonding to oxo ligands to form metal-oxygen motifs.[12] However, the deoxygenation process at high temperatures can render the reducible metal (hydr)oxides unstable, and metal ions may be reduced to neutral metal, which contaminates other metal sources.[38] The oxide form of inactive metal ions such as Al^{3+}, Ce^{4+} and Ti^{4+} of the support has better thermal stability than other reducible ones.[39, 40] In addition, due to their electrical conductivity and strong resistance to corrosion, metal nitrides/carbides, such as WC_X,[41] MoC,[42] TiN,[43] and MXene[44, 45] with metal centers exposed on their surface are good supports to stabilize single metal atoms through strong metal-metal interactions (**Figures 3a-3f**).

Recent studies have shown that atomic Co, Ni, and Pt on two-dimensional layered transition metal dichalcogenides (especially MoS_2) can enhance the catalytic activity.[46] Single metal atoms can be incorporated on 2D TMDs by doping, i.e., incorporation into the lattice, or by adsorption onto the surface.[47] Qi and collaborators reported the preparation of single-atom cobalt (Co) array covalently bound onto distorted 1T MoS_2 nanosheets *via* the strong Co-S covalent bonds through electrochemical cyclic voltammetry leaching of Co nanodisks (ND)-MoS_2 nanosheet hybrids (**Figures 3g-3j**).[48] The strain induced by the lattice mismatch and the formation of Co-S covalent bonds between Co and MoS_2 in the Co ND-MoS_2 nanosheet hybrids are shown to be critical to achieving the phase transformation of MoS_2 from the semiconducting 2H phase to the metallic distorted 1T phase.[49] The single-atom (SA) Co supported on distorted 1T MoS_2 catalyst exhibits Pt-like electrocatalytic activity for HER in the acid electrolyte and excellent long-term stability.

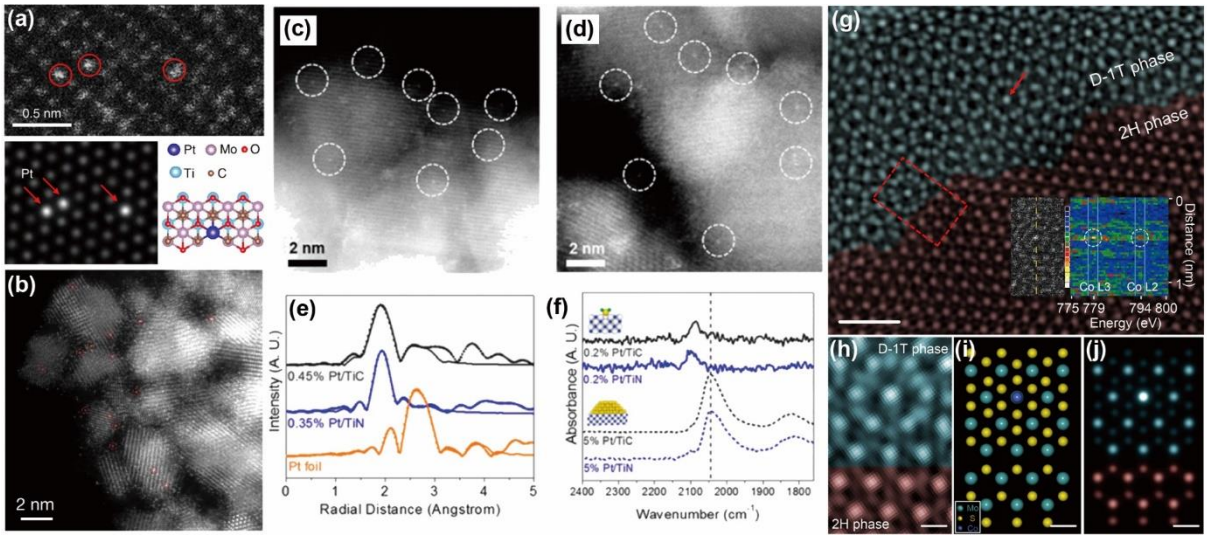

Figure 3 | Metal (hydr)oxides / nitrides / carbides / sulfide as supports for SACs. (a) HAADF-STEM image of Mo_2TiC_2Tx-Pt SACs and its corresponding simulated image. Reproduced from Ref. [39] with permission from Nature Publishing Group. (b) HAADF-STEM image of Pt/α-MoC with the single Pt atoms circled. Reproduced from Ref. [42] with permission from Nature Publishing Group. (c-f) Single-atom Pt loaded on TiC and TiN characterized by the HAADF-STEM, Pt L3 edge k^3 -weighted FT-EXAFS spectra and diffuse reflectance FT-IR spectra. Reproduced from Ref. [43] with permission from the American Chemical Society. (g-j) HAADF-STEM characterization of SA Co-D 1T MoS_2, which shows the obvious junction between SA Co-D 1T MoS_2 and pristine 2H MoS_2. Reproduced from Ref. [48] with permission from Nature Publishing Group.

Importance of the support in catalysis

Why metals as supports? Metals can be chosen as supports if the coordination and the electronic properties of the metal atoms need to be tuned. The advantages of metal supports are: (1) the fabrication methods for SAAs are usually easier to scale up and (2) the well-defined active sites in SAAs allow to understand and realize rational designs of SAAs using first principle calculations. The SAAs could tackle important challenges in industrial processes, such as for the selective hydrogenation of acetylene, the selective hydrogenation of 1,3-butadiene,[50] the formation of H_2 in methanol reforming[25] and also the methanol / ethanol oxidation reaction [51] by optimizing the binding energy of the reactants and the intermediates, leading to higher selectivity, stability, and resistance against poisoning (Table 1).

Why carbon-based materials as supports? Carbon-based materials as supports of SACs are interesting for applications where high surface area, high electronic conductivity and strong thermal stability are

needed. The metal atoms can be selectively trapped by the presence of carbon-heteroatoms (C-N, C-O, C-S and C-P) in order to better stabilize their atomic dispersion on the support. The local structure of metal-heteroatom (N, O, S and P)-carbon has been applied for various catalytic reactions, including the hydrogen evolution reaction,[52] in metal-air batteries,[55] the CO_2 reduction reaction,[56] the oxygen reduction reaction [62] and also the nitrogen fixation (Table 1).[63]

Why metal (hydr)oxides / nitrides / carbides / sulfides as supports? The coordination between supports and metal species induces strong interactions, inhibiting the aggregation of the metal atoms. Such supports typically offer high specific surface area, abundant metal or non-metal vacancies and surface functional groups to firmly anchor the single atoms. Significant charge transfer takes place between the single atoms and the support, which results in a charge redistribution from the neighboring nonmetallic atoms towards the metal atoms ultimately improving the catalytic property of the SACs. These supports have for example been used for the hydrodeoxygenation reaction,[67] peroxidase-like reactions,[69] the CO oxidation reaction [71] as well as the water-gas shift reaction (Table 1).[73]

Table 1

Compositions and applications of SACs with selected supports.

Support types	Supports	Single atoms	Applications	Refs
Metal	Cu (111)	Pt	Selective hydrogenation of 1,3-butadiene	[50]
Metal	Cu	Ag	H_2 formation in methanol reforming	[25]
Metal	Cu	Pt	Selective hydrogenation of acetylene	[53]
Metal	Pt nanowire	Ni	Methanol oxidation reaction Ethanol oxidation reaction	[51]
Carbon material	Graphdiyne	Pt	Hydrogen evolution reaction	[52]
Carbon material	S-doped carbon	Fe	Oxygen reduction reaction Oxygen evolution reaction Metal-air battery	[54, 55]
Carbon material	N-doped carbon	Pt, Ru, Fe, Co, Ni, Mo, Mn, Cu	CO_2 reduction reaction Oxygen reduction reaction Hydrogen evolution reaction	[56-64]

			Nitrogen fixation Metal-air battery	
Carbon material	N-doped carbon	Sn	CO_2 reduction reaction	[65]
Carbon material	Graphene	Co	Hydrogenation of nitroarenes	[66]
Metal sulfide	MoS_2	Co, Pt, Ni	Hydrodeoxygenation reaction Hydrogen evolution reaction	[67, 68]
Metal sulfide	MoS_2	Co	Peroxidase-like reaction	[69]
Metal carbide	MoC	Pt	Hydrogenation from water and methanol	[42]
Metal nitride	TiN	Pt	Oxygen reduction reaction	[70]
Metal (hydr)oxide	Al_2O_3	Pt	Hydrogenation reaction CO oxidation reaction	[20]
Metal (hydr)oxide	FeO_x	Pt, Ir	CO oxidation reaction Hydrogenation of nitroarenes Water-gas shift	[71-73]
Metal (hydr)oxide	ZnO	Rh	Hydroformylation of olefins	[74]
Metal (hydr)oxide	ZrO_2	Pd	Direct synthesis of indole	[75]
Metal (hydr)oxide	MgO	Ni	CO_2 reduction	[76]

Synthetic strategies of supported single atoms

An important principle for designing stable SACs is to construct strong interactions between isolated metal atoms and the underlying support. Exploration of synthesis methods has become an important research focus in the field of SACs.[77] However, because isolated single atoms can easily migrate and aggregate into particles because of their high surface energy,[78, 79] the fabrication of SACs under realistic synthesis and reaction conditions is challenging.[80] Mass-selected soft loading and atomic layer loading are two common approaches to fabricate SACs. These techniques can require costly

equipment, and the yield of single atoms is low. Therefore, alternative strategies for SACs have been pursued.[81] We review recent progress on the synthesis of SACs using some of these new approaches.

Wet chemistry

Wet chemistry involves mononuclear noble metal precursors to prepare SACs.[52, 82] Successful synthesis of SACs based on wet chemistry methods require: (i) low metal loading density to limit the aggregation and ensure atomic dispersion;[83] (ii) appropriate support that can anchor single atoms by forming sufficiently strong metal-support interactions.[84] Wet chemical methods commonly require a series of sequential steps, such as impregnation, coprecipitation, or deposition-precipitation, followed by calcination or reduction.[70, 85] The first step is used to anchor the metal atoms by regulating the interactions of the metal and support. The second step is to improve the metal-support interactions by modifying the electronic properties of the sites.

Zhang and coworkers successfully synthesized single-atom Pt_1/FeO_x catalysts with Pt loading of 0.17 wt.% through a coprecipitation method (**Figure 4a and 4b**).[71] At higher loading concentration of 2.5 wt.%, they observed Pt clusters. Density functional theory (DFT) studies show that the electronic interactions between Pt atoms and FeO_x can generate vacant 5d orbitals of the positively charged Pt atoms, which are helpful for strong binding and stabilization of single Pt atoms and responsible for the improved catalytic activity towards CO oxidation. Single-atom Pt was also prepared *via* calcination and demonstrated outstanding stability towards 1,3-the butadiene hydrogenation and n-hexane reforming reactions under demanding conditions (**Figure 4c**).[86] The Pt atoms were firmly anchored on the internal surfaces of mesoporous Al_2O_3, which is likely stabilized by unsaturated pentahedral Al^{3+} centers. Room-temperature photochemical strategy to fabricate highly stable, atomically dispersed Pd catalyst (Pd_1/TiO_2) on ultrathin TiO_2 nanosheets with Pd loading up to 1.5 wt.% has been

demonstrated.[87] Ultraviolet-light-induced formation of ethylene glycolate radicals on TiO_2 nanosheets was demonstrated to be critical for preparing Pd SACs supported on TiO_2: Pd_1/TiO_2. Alternatively, Pd_1/TiO_2 was continuously prepared using a peristaltic pump and UV-flow reactor, which made the process compatible for a large-scale production of SACs (**Figure 4d**). Recently, Wu and coworkers developed a facile approach to generate atomically dispersed Pt *via* photochemical reduction of frozen chloroplatinic acid solution using ultraviolet light irradiation.[88] Using this iced-photochemical reduction, the aggregation of atoms is prevented, and single atoms are successfully stabilized as illustrated in **Figure 4e**. Most importantly, the obtained metal single atoms can be anchored on various supports, including mesoporous carbon, graphene, carbon nanotubes, titanium dioxide nanoparticles, and zinc oxide nanowire, which expands the routes for the wet synthesis of SACs and their intrinsic activities.

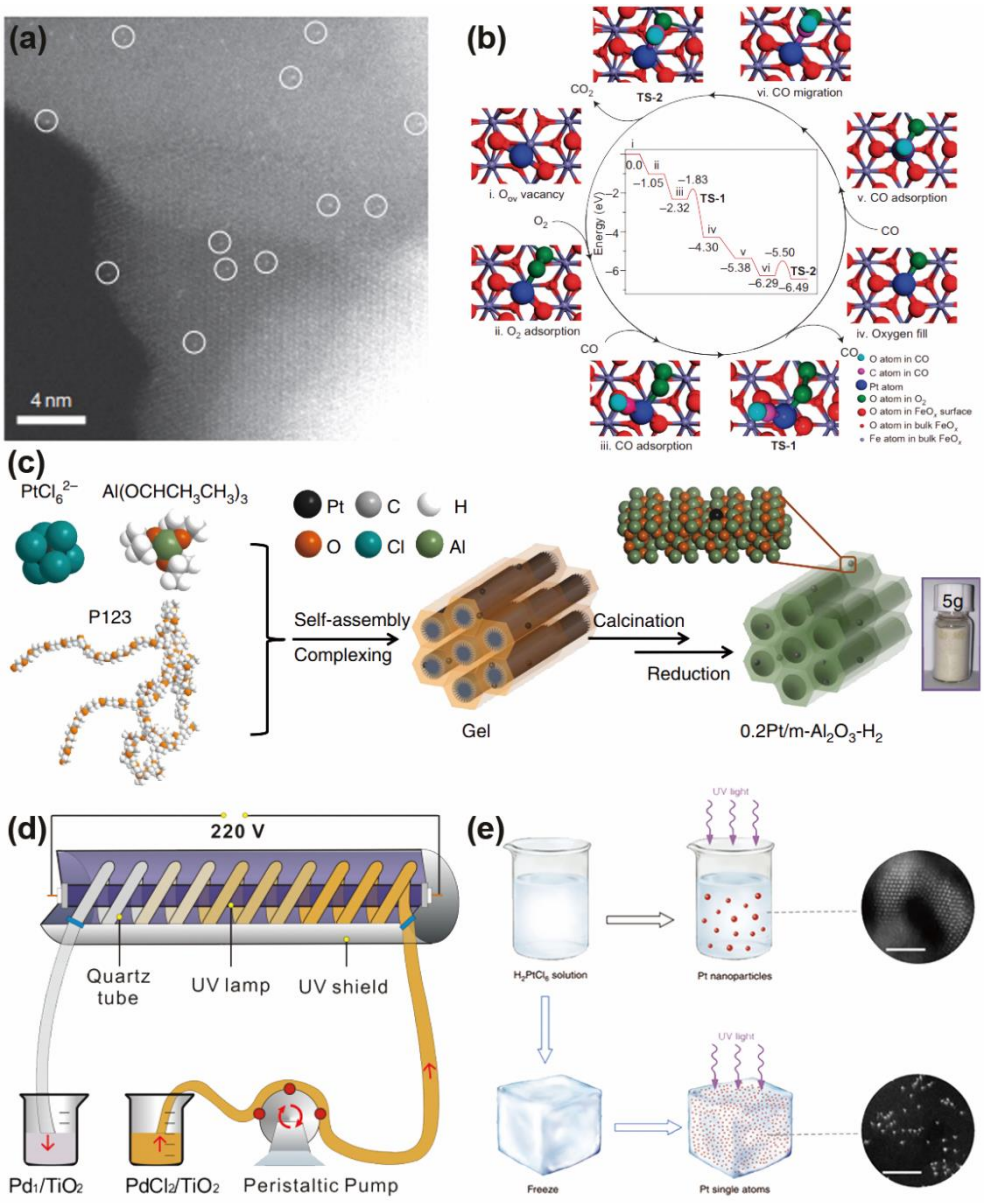

Figure 4 | Wet chemistry methods for the synthesis of SACs. (a) HAADF-STEM characterization of SACs and (b) proposed reaction pathways for CO oxidation on Pt_1/FeO_x. Reproduced from Ref. [71] with permission from Nature Publishing Group. (c) Schematic illustration of the Pt/m-Al_2O_3-H_2 synthesis process. Reproduced from Ref. [86] with permission from Nature Publishing Group. (d) Wet chemical preparation of Pd_1/TiO_2 in large scale. Using a peristaltic pump and UV-flow reactor, Pd_1/TiO_2 was continuously prepared. Reproduced from Ref. [87] with permission from AAAS. (e) Schematic illustration of the iced-photochemical process: freezing the precursor before exposing it to UV irradiation and obtaining Pt single atoms dispersed in ice. The ice lattice naturally confined the ions/atoms and prevented their nucleation. Reproduced from Ref. [88] with permission from Nature Publishing Group.

Defect engineering

The defect engineering strategy represents an efficient method to tune the electronic structure and surface morphology.[89, 90] Defect engineering uses the defects on the support to trap metal precursors and stabilize isolated metal atoms against sintering via charge transfer between single atoms and defective sites.[91] In this approach, it is important to optimize the conditions to ensure the formation of uniformly dispersed defective centers on the support. Atomic defects in the form of vacancies perturb the local electronic structure and coordination environment, which can stabilize single atoms.[92, 93] These defects on the supports can serve as ‘‘traps’’ to capture metal precursors and anchor metal atoms during posttreatment.

Among different types of defects, cation vacancies have recently been exploited to synthesize SACs.[94] **Figure 5a** shows single Au atomic site supported on defective TiO_2 nanosheets. Surface defects on TiO_2 nanosheets have been found to effectively stabilize Au single atoms through formation of Ti-Au-Ti bonds, which promote the catalytic performance by reducing the energy barrier and optimizing the CO adsorption on isolated Au sites.[93] Pt SACs with Pt loading as high as 2.3 wt.% have been synthesized by employing defect-rich nickel hydroxide nanosheets with abundant Ni^{2+} vacancies as the support (**Figure 5b**).[95] X-ray absorption spectrometry analyses and DFT calculations reveal that the high metal loading and excellent stability of single Pt atoms are ascribed to the stabilization effects of Ni vacancies as anchoring sites *via* charge transfer.

The important role of sulfur vacancies in the formation of isolated metal atoms against sintering has been recently revealed.[96] For example, sulfur vacancies frequently exist in layered transition metal dichalcogenides, such as MoS_2 and WS_2.[97] Exfoliated MoS_2 monolayers are typically rich in sulfur vacancies on the basal plane, which are formed during the Li^+ intercalation and chemical exfoliation

processes.[98] As illustrated in **Figure 5c**, S-deficient MoS_2 layers can trap and bind thiourea-based Co species with high affinity by refilling the S vacancies to obtain isolated Co atoms dispersed on MoS_2 monolayers. Experiments and DFT calculations revealed unexpectedly high activity and excellent stability with limited sulfur stripping. The excellent performance is attributed to the strong covalent attachment of Co atoms on monolayer MoS_2 and the presence of Co-S-Mo interfacial sites, which are formed on S vacancy sites. Alternatively, the single sulfur vacancy has recently been identified as an active site for the evolution of hydrogen by itself. The controlled formation of sulfur vacancies causes a turnover frequency of 5 s^{-1} at 0 V overpotential.[99]

Carbon vacancies often appear in carbon-based materials and can serve as anchoring sites for single metal atoms via electron transfer.[100] Chisholm and coworkers reported a catalytically active Nb catalyst in the form of isolated Nb atoms in onion-like carbon shells.[101] Theoretical calculations demonstrate that the tri-vacancy sites in the carbon layer are the most energetically favorable for anchoring Nb atoms (**Figure 5d**). The enhanced electronic conductivity and chemical stability are attributed to the redistribution of *d*-band electrons of Nb atoms inserted inside the carbon lattice. Similarly, the activation and stabilization of single Ni atoms in both acid and alkaline electrolyte have been ascribed to the charge transfer between Ni atoms and the surrounding C atoms (**Figure 5e**).[102]

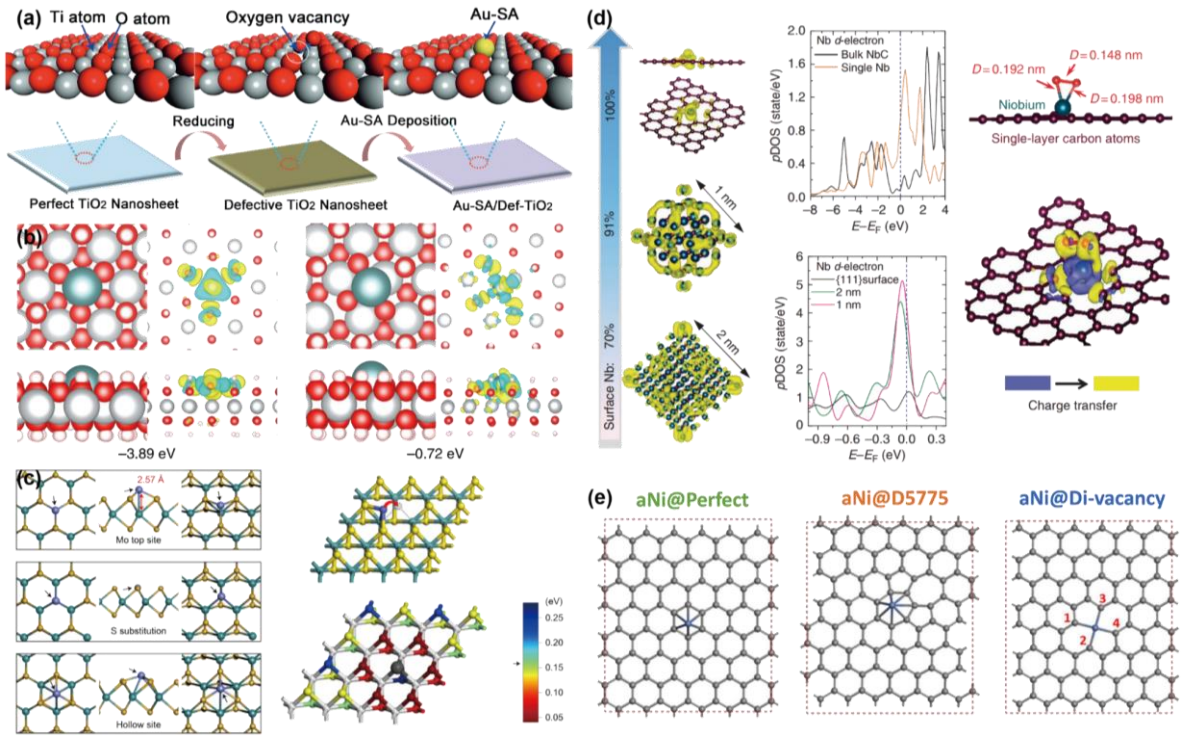

Figure 5 | Defect engineering strategy for the synthesis of SACs. (a) Synthesis process for isolated Au atoms stabilized on defective TiO_2 nanosheets with oxygen vacancies or defects. Reproduced from Ref. [93] with permission from Wiley. (b) The most stable configuration and charge density difference of a single Pt atom trapped on $Ni(OH)_2$ nanosheets with abundant Ni^{2+} vacancies by DFT calculations. Reproduced from Ref. [95] with permission from Nature Publishing Group. (c) DFT optimized geometries of three Co binding configurations and the energetics of how the Co-S-Mo interface promotes the formation of more sulfur vacancy sites. Reproduced from Ref. [98] with permission from Nature Publishing Group. (d) Theoretical simulations of the catalytic origins. Isosurface of the charge-density distribution and *d*-electron DOS for the niobium atoms at the corner of clusters and the doped single niobium atom. Reproduced from Ref. [101] with permission from Nature Publishing Group. (e) Illustrations of three different types of catalytic active sites corresponding to a single Ni atom supported on carbon sites. Reproduced from Ref. [102] with permission from Elsevier.

Spatial confinement

Alternatively, to defect engineering and wet strategies, which rely on chemical interactions with the support, single metal atoms can be confined into molecular-scale cages to prevent aggregation. The synthetic strategy for spatial confinement of SAs is a two-step process. The first step consists of achieving high spatial distribution and atomic dispersion of metal species by separating and

encapsulating suitable mononuclear metal precursors using porous materials such as metal-organic framework (MOFs) and covalent-organic frameworks (COFs). Then, a posttreatment enables the removal or conversion of the precursor ligands and the formation of single metal atoms stabilized on the support.[103] This versatile strategy has led to the development of SACs based on various metals and supports. MOFs have become tunable and versatile platforms for single-atom catalysis because they have abundant intrinsic molecular metal sites, large surface area, ordered pore structure and chemical robustness. The MOF support can also provide complementary properties to the SAs. For example, single metal atoms confined in MOFs have been used for the photocatalytic production to produce hydrogen under visible light irradiation (**Figure 6a**).[104] The electron transfer from the MOF photosensitizer to the Pt SA sites enabled the production of hydrogen from water splitting under visible light irradiation. The single Pt atoms exhibited outstanding photocatalytic activity with a turnover frequency of 35 h^{-1}, which is ~30 times that of Pt nanoparticles in the same configuration. Ultrafast transient absorption spectroscopy unveiled that single Pt atoms confined in MOF provided highly efficient electron transfer channels, while density functional theory calculations indicated that the introduction of single Pt atoms into MOF improved the hydrogen binding energy, which strongly boosted the photocatalytic H_2 production activity.

Due to a porous structure, a metal organic framework has been used as the host to confine metal atoms or their precursors. In particular, zeolitic imidazolate frameworks (ZIF) based on zinc are particularly interesting because zinc vaporizes upon thermal annealing, which leaves only the metal atoms in the form of clusters and individual atoms on the support. Extensive acid washing is typically required to remove the aggregated metal atoms. MOF-derived SACs can also be prepared using nitrogen-based ligands, which have the advantage of doping the final carbon support with nitrogen atoms upon

graphitization. The doping of the carbon support has been utilized to anchor highly mobile metal atoms and stabilize single atoms during pyrolysis by forming strong metal-nitrogen coordination bonds to prevent aggregation.[105] This approach has notably been used to prepare Fe and Co SAs dispersed on nitrogen-doped carbon support: Fe-C-N and Co-C-N.[106] In this context, Wang and coworkers have developed an original host-guest strategy to construct an electrocatalyst with Fe-Co dual sites embedded within N-doped porous carbon (**Figure 6b**).[107] The Fe and Co ionic precursors were trapped in the structure of a ZIF-8 MOF. The (Fe, Co)/N-C SACs exhibit superior oxygen reduction reaction performance in acidic electrolyte with comparable onset potential and half-wave potential to commercial Pt/C. The spatially confined dual sites favor the activation of O-O, which is a key elementary step to reduce oxygen *via* the four-electron mechanism. The metal precursors can directly be used in the MOF structure and further converted to SA sites. For example, SACs with atomically dispersed Ru-N-C sites have been prepared from MOF *via* the two-step synthetic strategy. With the assistance of uncoordinated amine groups in the terephthalic acid as linkers, Ru ions were coordinated and confined in the skeletons of UiO-66-NH_2, which effectively inhibited the migration of Ru species (**Figure 6c**).[108] These single Ru sites with single-mind N coordination can serve as a semihomogeneous catalyst to effectively catalyze the chemoselective hydrogenation of functionalized quinolones.

The porous structure of MOFs can also be used to encapsulate metal nanoparticles that are further transformed into dispersed individual atoms. Using such synthetic route, Li's groups investigated the dynamic conversion of metal nanoparticles (Pd, Pt or Au) trapped inside a ZIF template into thermally stable single atoms (Pd, Pt, Au-SAs) above 900 °C in an inert atmosphere (**Figure 6d**).[109] The dynamic process recorded by *in situ* environmental transmission electron microscopy revealed

competing sintering and atomization processes during the NP-to-SA conversion. Density functional theory calculations showed that the high-temperature NP-to-SA conversion was driven by the formation of thermodynamically stable Pd-N_4 structure. and the mobile Pd atoms were captured on defects of nitrogen-doped carbon. The thermally stable single atoms (Pd-SAs) outperformed Pd nanoparticles for the semihydrogenation of acetylene.

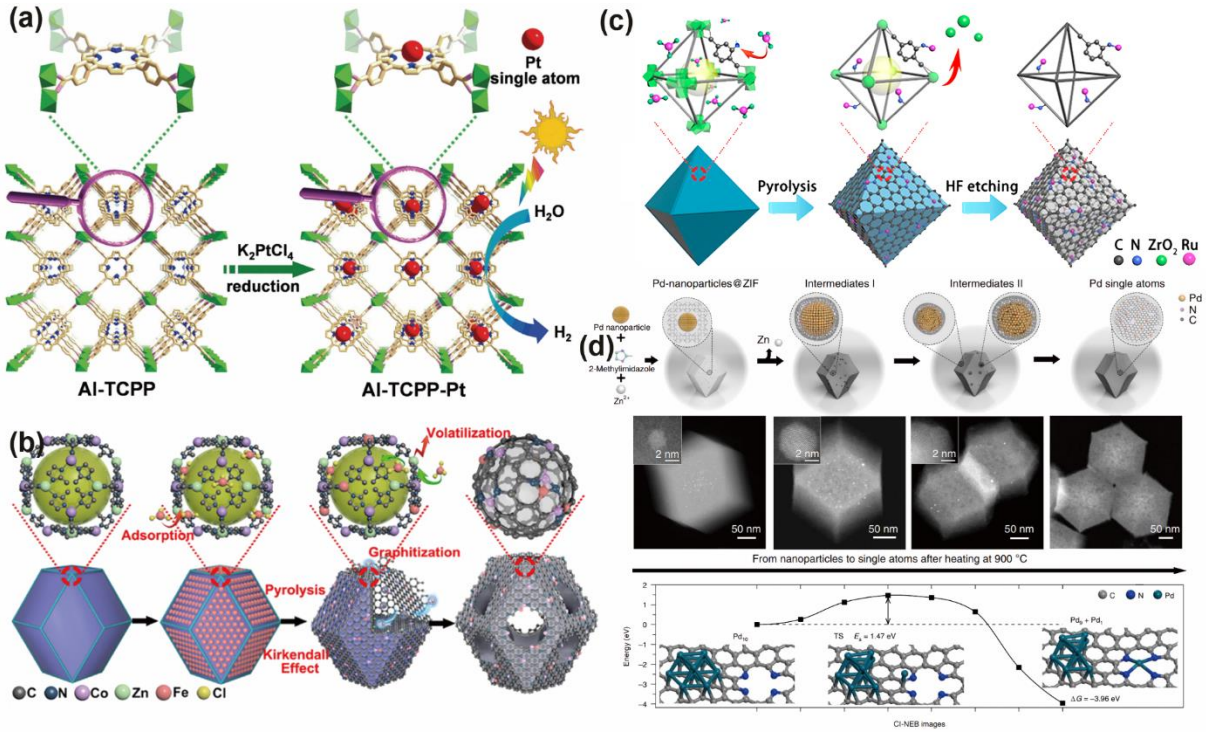

Figure 6 | Spatially confining strategy for the synthesis of SACs. (a) Schematic illustration of the synthesis of Al-TCPP-Pt for photocatalytic hydrogen production. Reproduced from Ref. [104] with permission from Wiley. (b) Preparation diagram of (Fe,Co)/N-C. Reproduced from Ref. [107] with permission from the American Chemical Society. (c) Scheme of the proposed formation mechanisms for Ru SA. Reproduced from Ref. [108] with permission from the American Chemical Society. (d) Scheme of the transformation of nanoparticles to single atoms, structural characterizations of Pd single atoms and Calculated energies along the stretching pathway of the Pd atom from the Pd_{10} cluster to Pd-N_4 defect by CI-NEB, and the corresponding initial and final configurations. Pd, green; C, gray; N, blue. Reproduced from Ref. [109] with permission from Nature Publishing Group.

Coordination design between the support and the single-atom sites

The rational design of coordination sites has been explored to adsorb and bind metal precursors or metal atoms while preventing the migration and agglomeration of the SAs.[16]_For example, coordinating atoms, such as N, O, and S, enable strong interactions with metal atoms due to the lone pair electrons that promote the preparation of SACs with these coordinating atoms as anchoring sites.[55, 63] Similar to defect engineering, uniform coordination sites on the support should be prepared prior to the incorporation of single metal atoms to form homogeneous active centers. The mononuclear metal precursors are adsorbed and bound to the coordination sites, which prevent their migration and agglomeration during the posttreatment process. Selecting suitable mononuclear metal precursors that can strongly interact with the coordination sites is critical. Therefore, maintaining strong interactions between the coordinating atoms and the single metal atoms during the entire synthesis process is important. The ability of coordinating atoms to bind with metal atoms is affected by the synthesis conditions such as the solution pH and nature of the solvents. The precise control of synthesis conditions is necessary for successful synthesis of SACs. Due to strong interactions with coordinating atoms on the supports, the as-formed single metal atoms tend to exhibit higher stability than those SACs synthesized by traditional wet-chemistry methods. Moreover, the electronic structure of single-atom active centers can be modified by the surrounding coordination atoms, which results in tunable catalytic performance.[110]

In the case of single-layer graphene as the support, different coordination environments have been proposed, including single vacancies with three carbon atoms, double vacancies with four carbon atoms, four pyridine nitrogen atoms and four pyrrole nitrogen atoms (**Figure 7a**).[111] The catalytic activity of the single-atom sites on the graphene support is highly correlated with the local environment of the metal center, i.e., its coordination number and electronegativity of nearest-neighbor atoms.[112]

Bimetallic Co/Zn ZIFs have been prepared by replacing some of the Zn atoms with Co (**Figure 7b**).[113] After pyrolysis, the Zn atoms evaporate, and the Co nodes are reduced *in situ* to form single Co atoms stabilized *via* the strong interaction between the N and Co atoms. Huang and coworkers reported a general approach to synthesize a series of atomic transition metals (e.g., Fe, Co, or Ni) dispersed on a nitrogen-doped graphene matrix with a definitive MN_4C_4 moiety (**Figure 7c**).[114] Nitrogen-doped graphene supports were prepared by annealing pristine graphene in ammonia atmosphere to coordinate and stabilize the metal atoms. Li and coauthors demonstrated a large-scale synthesis strategy of single-atom catalysts *via* direct atom emission from bulk metals followed by trapping on nitrogen-rich porous carbon obtained using ammonia.[115] In this synthetic strategy, as shown in **Figure 7d**, ammonia first coordinates with metal atoms such as Cu to form volatile $Cu(NH_3)_x$ species due to the strong Lewis acid-base interactions. Then, these species are transported using ammonia as the carrier gas before adsorbing on defect sites of carbon support and forming abundant isolated copper SA sites.

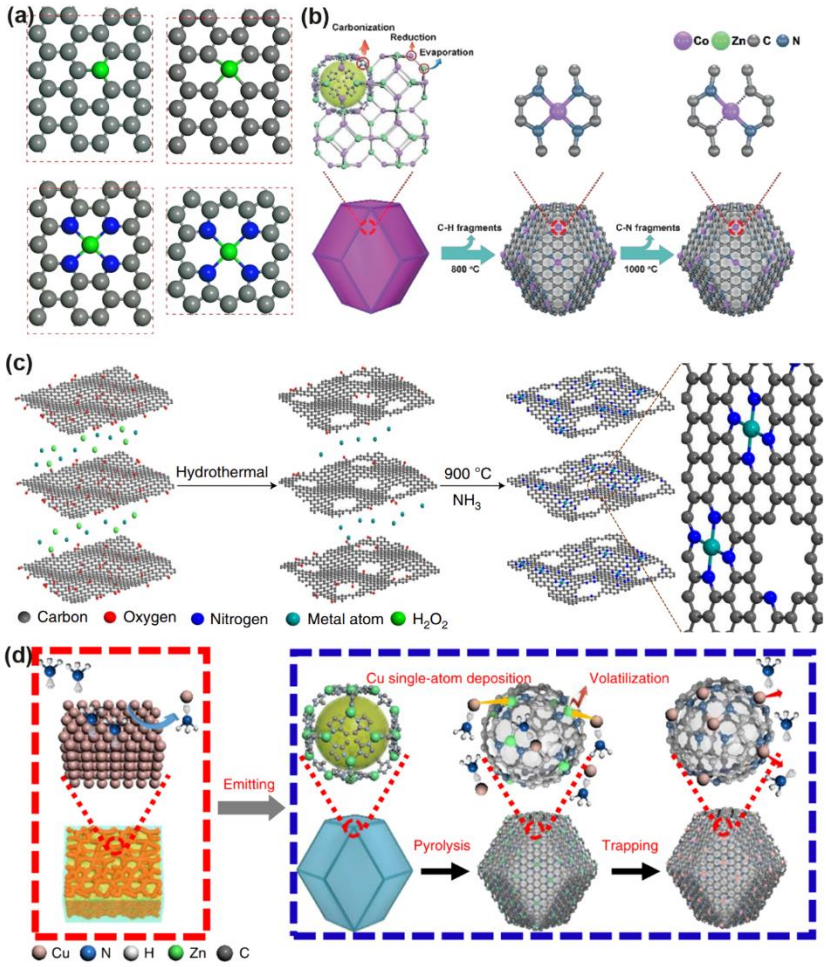

Figure 7 | Coordination design strategy to synthesize SACs. (a) Schematic of a single metal atom supported on graphene with different coordination environments. The green, blue and gray colors represent metal, nitrogen and carbon atoms, respectively. Reproduced from Ref. [111] with permission from Nature Publishing Group. (b) Formation process of Co-N_4 and Co-N_2. Reproduced from Ref. [113] with permission from Wiley. (c) Preparation route of M-NHGFs. The graphene oxide solution in the presence of H_2O_2 and metal precursors was hydrothermally treated to form a 3D graphene hydrogel. After freeze-drying the hydrogel, one used a thermal annealing process in an NH_3 atmosphere to further reduce the graphene and incorporate N-dopants into the 2D graphene lattice. Reproduced from Ref. [114] with permission from Nature Publishing Group. (d) Schematic and the proposed reaction mechanism to prepare Cu-SAs/N-C. Reproduced from Ref. [115] with permission from Nature Publishing Group.

Physical characterization of the single-atom-support interactions

The identification of atomically dispersed metals and determination of their distributions with their coordinating environments and metal-support interactions are critical for investigating metal

SACs.[116] Characterization techniques such as high-resolution electron microscopy and X-ray spectroscopy have been used to study SACs. Due to the “Z” contrast from the atomic number of chemical elements, aberration-corrected high-angle annular dark-field scanning transmission electron microscopy (HAADF-STEM) is particularly suited for direct observation of the SAs.[117] In parallel, the development of X-ray absorption spectroscopy (XAS) including extended X-ray absorption fine structure (EXAFS) and X-ray absorption near-edge structure spectroscopy (XANES) enables access to the local structure of single atoms on supports by elucidating the coordination and electronic structure of SAs.[118] A generally accepted analysis procedure to confirm the presence of single metal atoms consists of EXAFS measurements coupled with XANES measurements. The spectrum fitting enables the determination and quantification of the coordination environment of the SAs.

Extended X-ray absorption fine structure (EXAFS)

EXAFS spectra arise from the interference effects between outgoing wave and back-scattered wave produced by the surrounding atoms around the central atom. It provides an average information over the probed regions.[119] The EXAFS analysis allows access to the local coordination number, interatomic distances, structural disorder, and neighboring atoms over different bond lengths.[120] For SACs, the absence of metal-metal bonding in the EXAFS spectra is a positive signature of isolated metal atoms. Meanwhile, XANES enables us to probe the electronic and geometric coordination structures of metal species based on the white-line intensity with the peak features. A combination of EXAFS and XANES has been used to determine the local interactions between the metal atoms and the support for M-C-N (M=FE, Co). For example, Chen and coauthors have used EXAFS measurements to elucidate the interactions between the Fe-N_4 single atom and the nitrogen-doped

porous carbon (NPC) support.[121] From the Fe K-edge spectrum, the absorption threshold position of Fe SA was identified to be between the FeO and Fe_2O_3 features, which indicates that the valence state of Fe in FeN_4 SAs/NPC is situated between +2 and +3 (**Figure 8a**). From the Fourier transformed (FT) k^3-weighted EXAFS (**Figure 8b**), the main peak at 1.4 Å corresponds to the Fe-N first coordination shell. Compared with Fe foil, FeO and Fe_2O_3, no Fe-Fe coordination peak at 2.2 Å is detected, which demonstrates the atomic dispersion of Fe.[122] Only one intensity maximum at ~ 4 $Å^{-1}$ is observed from the wavelet transform (WT) contour plots of Fe-N_4 SAs/NPC, which can be assigned to the Fe-N coordination. The XAFS fitting indicates that the first shell of the Fe atom shows a coordination number of 4, which is consistent with the presence of 4 coordinating nitrogen atoms (inset of **Figure 8a**). Similar results that suggest the coordination of metal atoms to the support using 4 nitrogen atoms have been lately proposed for Pd, Co, etc.[123, 124]

To obtain a deeper insight on the SA sites, it is necessary to perform EXAFS and XANES on different reference samples with different coordinating environments for the metal atoms. Liu and coworkers used EXAFS to study Ni SAs supported on N-doped graphene.[125] As expected, the peak at 2.15 Å for the Ni-Ni interaction in Ni nanoparticles and Ni foil was not observed, and the main peak at approximately 1.45 Å is attributed to the scattering interaction between Ni atoms and NiN. An additional small peak appears at 1.81 Å for Ni SAs supported on N-, S-doped graphene, which is approximately 0.36 Å larger than the Ni-N distance and is consistent with the longer Ni-S bond length.[126] Similarly, **Figures 8e-8g** show the structural and electronic states of the single-atom Co supported on graphene: labeled as Co_1/G SACs with different loading amounts in the figures.[66] Meanwhile, the XANES white line peaks of Co_1/G SACs samples with different loadings are centered at 7727.1 eV, between those of Co foil (7725.7 eV) and Co_3O_4 (7728.0 eV), which suggests that the

as-prepared Co SAs are in the oxidized state instead of the metallic state. Additional structural information can be explicitly inferred from the EXAFS spectra at the Co K-edge (**Figure 8g**). Notably, a shorter bond is observed in the case of Co_1/G SACs: 1.56 Å compared to the bonds for the $CoCp_2$ molecule and chemisorbed $CoCp_2$ precursors on graphene at 1.60 Å and 1.58 Å, respectively, which shows the particular configuration of the Co SAs.

Single atoms can have different coordination environments that will translate into different electronic and catalytic behaviors. It is therefore highly important to precisely determine the coordination of the single atoms on the support. According to the literature, the coordination environment is strongly related to the synthesis environment or synthesis process; in particular the pyrolysis temperature and the M_1/M_2 atomic ratios (M_1 and M_2 refer to the single metal atom and metal support respectively). XANES can provide valuable information regarding the oxidation degree and valence state of the SACs, while EXAFS is found to be sensitive to the coordination environment of the single-atoms. Combination of both techniques can allow to distinguish the different coordination. However, this requires the use of reference samples and proper fitting the spectra. For example, Wang et al. used EXAFS and XANES to elucidate the coordination environment of SA Co sites.[114] The XANES spectra between Co-N_2 and Co-N_4 shows a progressive shift towards the lower energy suggesting a reduction of the oxidation degree for the Co atoms. In R space, the EXAFS spectra of Co-N_x exhibit a prominent peak at ca. 1.4 Å from the Co-N coordination and the intensity of Co-N peak for Co-N_2 is much lower than that of Co-N_3 and Co-N_4, which implies a reduction of the number of N atoms surrounding the center Co.

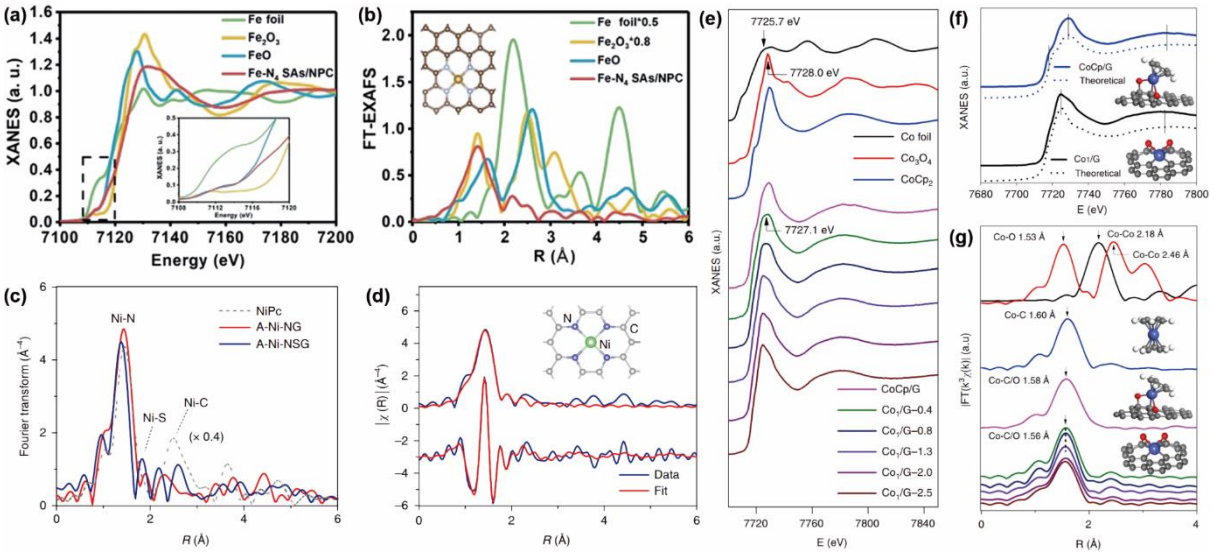

Figure 8 | X-ray absorption fine structure characterization of SACs. (a-b) XANES of Fe K-edge and FT at R space (inset: Fe atomic structure model; C gold, N silver, and Fe orange). Reproduced from Ref. [121] with permission from Wiley. (c-d) Fourier transformation of the EXAFS spectra, where the NiPc spectrum has been reduced in size; First-shell (Ni–N) fitting of Fourier transformations of EXAFS spectra for A-Ni-NG. The top and bottom traces are the magnitude and imaginary part, respectively. Reproduced from Ref. [125] with permission from Nature Publishing Group. (e-g) Co K-edge XAFS and EXAFS spectra of CoCp/G, Co_1/G SACs. Reproduced from Ref. [66] with permission from Nature Publishing Group.

High-resolution electron microscopy

Progress in electron microscopy has allowed direct observation of individual atoms on supports, and this technique is now widely applied to characterize metal SACs.[24] When metal atoms are significantly heavier than support atoms, it is possible to detect their position and distribution *via* high-angle annular dark-field electron microscopy scanning transmission (HAADF - STEM).[127] HAADF - STEM provides insight to discriminate pure single metal atoms from metal clusters and nanoparticles by allowing the identification and spatial distribution of single atom on the support. HAADF-STEM has been recently used to observe the atomic structure of series of 3*d* metal single atoms embedded in nitrogen-doped holey graphene frameworks (M-NHGFs, M=Fe, Co or Ni)

(**Figure 9a**).[114] The images revealed a uniform dispersion of heavy metal atoms, which are observed as bright dots, almost exclusively as single atoms throughout the graphene matrix. The atomic structure within the single-layer graphene support was clearly resolved, while coordination configurations of SAs match well with MN_4C_4 moieties predicted from XAFS measurements. Remarkably, HAADF-STEM also allows the identification arrangement of light elements near metal sites and distortion of the graphene honeycomb lattice structure.[128] For example, the presence of such distortions can reveal the existence of pyrrolic or pyridinic-N-based structures for SAs in the graphene matrix.[129, 130] Beyond the carbon-based support, HAADF-STEM has been used to characterize the coordination environment of other types of SACs. Tsang *et al.* used HAADF-STEM to prove that atomic Co could form at sites beyond Mo atop MoS_2 and edge sites.[131] The characteristic hexagonal pattern of alternating intensity spots associated with 2H MoS_2 monolayer is shown in **Figure 9b**. The intensity profile analysis of the HAADF images demonstrates that in addition to Co on basal plane Mo sites, there is evidence for Co being substituted for sulfur. Co atoms were also observed occupying positions at the center of MoS_2 hexagons. The three observed configurations for Co SAs on the MoS_2 basal plane were predicted to be the most energy-favorable geometries by DFT. This result demonstrates how the high-resolution microscopy and numerical simulations can be used in complementary fashion (**Figure 9c**). Li and coworkers observed the single-atom distribution using the HAADF line scanning profile of Co-substituted Ru nanosheets (NSs) (**Figure 9d**).[132] The presence of Co SAs was also supported by the electron energy loss spectroscopy (EELS) spectra of Co K-edges from three atomic column locations (**Figure 9d, e**).

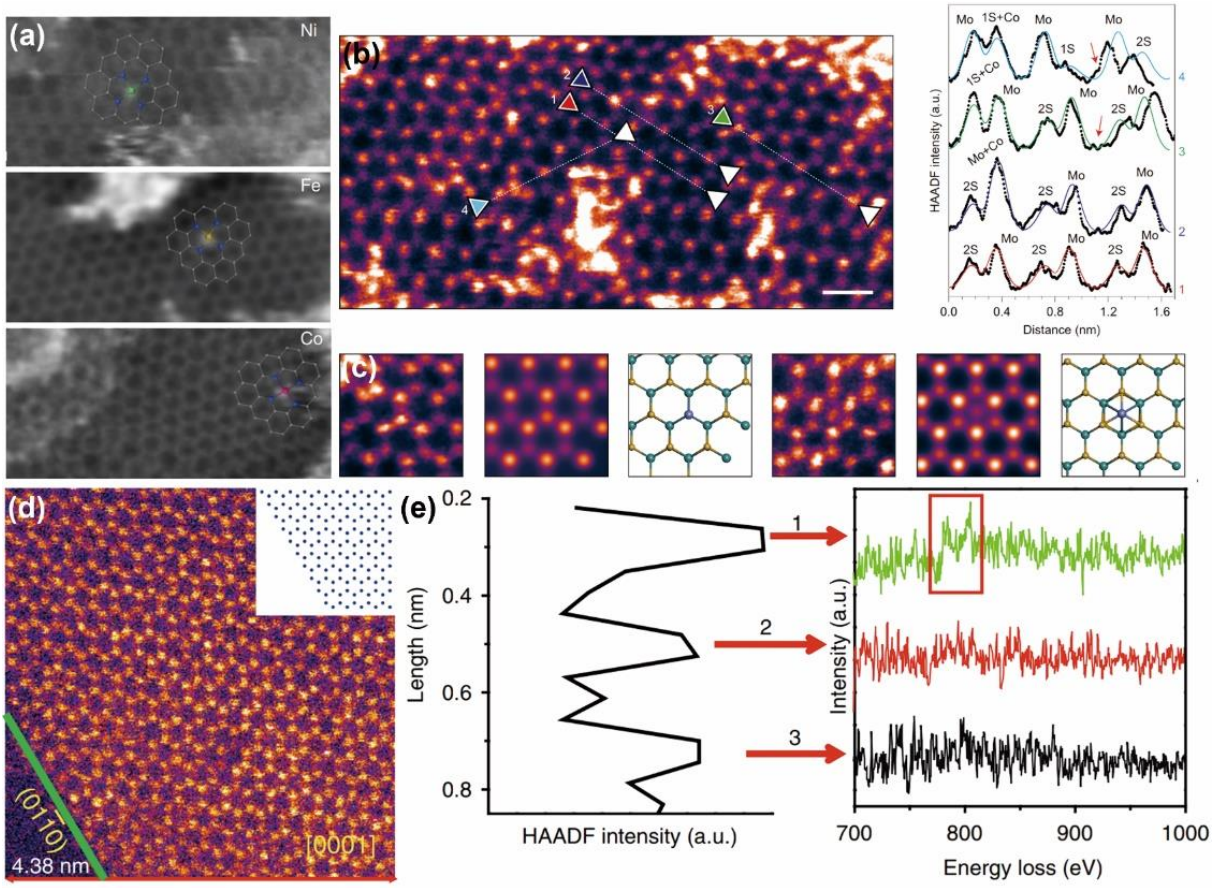

Figure 9 | Electron microscopy imaging characterization of SACs (a) Atomic structure characterizations of M-NHGFs by HAADF-STEM that enable the direct visualization of atomic metals of Ni, Fe and Co embedded in the 2D graphene lattice. The overlaid schematics represent the structural models determined from the XAFS analysis. Reproduced from Ref. [114] with permission from Nature Publishing Group. (b) Detailed atomic resolution HAADF-STEM characterization of the basal plane of used Co-MoS_2; the image simulation and atomic model are also provided. Reproduced from Ref. [133] with permission from Nature Publishing Group. (c) HAADF image, atomic model and DFT optimized geometry for Co-substituted S site and Co in the hollow site. (d) Atomic resolution HAADF-STEM image of a single Co-substituted Ru nanosheet. (e) Line scanning profile and background-subtracted EELS spectrum of the Co-substituted Ru NSs. Reproduced from Ref. [132] with permission from Nature Publishing Group.

Scanning tunneling microscopy

Atomic-resolution scanning tunneling microscopy (STM) is an excellent technique to study individual metal atoms and probe the local electronic structure.[134, 135] For example, Lucci et al. used STM to successfully identify single Pt atoms supported on Cu(111) surfaces.[50] The obtained STM images

revealed that Pt atoms were incorporated directly into Cu(111) terraces and in the areas above the surface step edges through place exchange (**Figure 10a, b**). The main advantage of STM imaging is the ability to visualize atomic-scale structure on the surface around the single atoms during reactions, which enables to explore of the reaction mechanisms and sintering of the single atoms. STM can not only image individual metal atoms but also probe the nature of the reactant molecular adsorption sites. Liu et al. explored the interactions of CO and H with Pt single-atom active sites on Pt-Cu (111) SAA surfaces using STM (**Figure 10c-10e**). They notably observed the selective adsorption of CO onto Pt sites while H adatoms are capable of diffusing into Cu sites far from the Pt dissociation sites during the hydrogen electro-oxidation.[53]

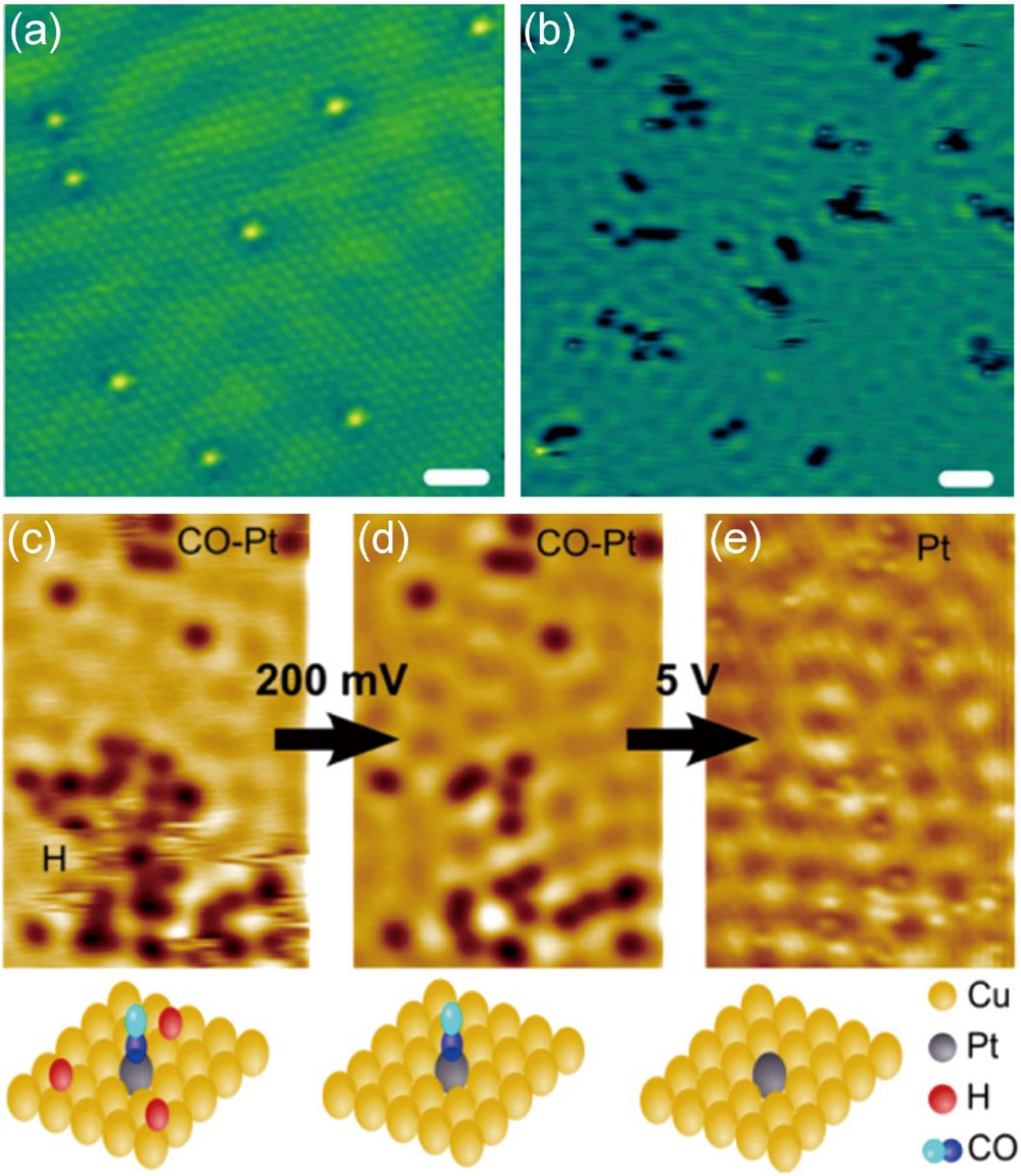

Figure 10 | Scanning tunneling microscopy characterization of SACs (a) STM image of 0.02 ml Pt/Cu (111) SAA surface in which Pt atoms appear as isolated protrusions on the Cu (111) surface. (b) STM image showing H atom spillover onto Cu. H atoms appear as depressions and form small mobile clusters. Reproduced from Ref.[50] with permission from Nature Publishing Group. (c-e) STM images showing the co-adsorption of H and CO on a Pt-Cu (111) SAA surface and STM tip-induced adsorbate removal to reveal the binding sites underneath. Reproduced from Ref. [53] with permission from the American Chemical Society.

Atom probe tomography

Atom probe tomography (APT) is a characterization technique that allows both atomic-level three-dimensional (3D) imaging and probing the chemical composition.[136] Under laser or HV pulsing, the atoms are evaporated in the form of ions from the surface of the SACs and projected onto a position-sensitive detector (PSD) with a very high detection efficiency. Measuring the time of arrival of the ions on the PSD allows to determine the mass over charge (m/q) ratio. The X-Y position and the order of arrival for the ions on the PSD enable to reconstruct the original position of the atoms. Wang et al. used the APT to characterize single-atom Fe immobilized on carbon nanotubes (CNTs).[137] As demonstrated in **Figure 11a**, the 3D reconstructed tomography image of the specimen is obtained by collecting 9 million atoms, and the projected 2D image is shown in **Figure 11b**. Each green dot represents an isolated single Fe atom, which is randomly dispersed in the carbon support (**Figure 11c-11d**). The side and top view of the CNTs shows that the single Fe atoms may bind with neighboring C and O atoms, indicating the possible coordination of the Fe-C-O center. Although the APT cannot provide an exact atomic structure of the isolated single atoms due to the loss of the ionic signals during the detection process, the technique can help identify the possible coordination environment of SACs. For example, Wang et al. synthesized Ni single atoms coordinated in a graphene shell for the aqueous CO_2 electroreduction to CO and conducted APT to elucidate the atomic structure of the Ni sites.[138] The APT results showed that only 0.2% of the Ni single atoms are directly coordinated with N atoms (**Figure 11e-11g**). Combined with DFT calculations, the APT suggested that the Ni atoms coordinated in the graphene vacancies are the major active sites for the electrocatalytic CO_2 reduction to CO rather than the Ni-N species. APT can therefore serve as a powerful complementary characterization technique to STEM and XAS to provide information on the real atomic structure of the catalytically active sites.[139]

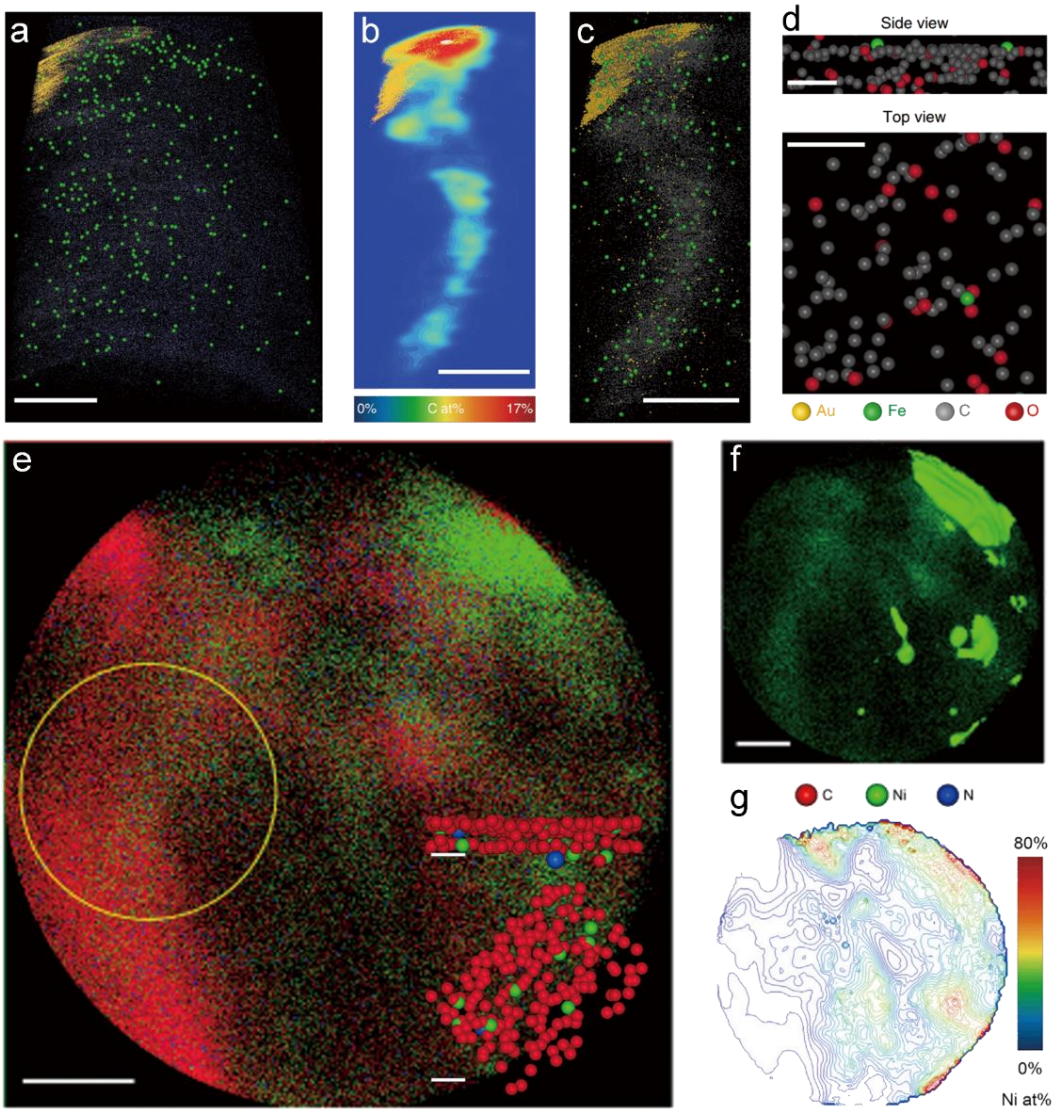

Figure 11 | Atom probe tomography characterization of SACs (a) Reconstructed APT data from Fe SAs supported on CNTs, with (b) a 2D contour plot of the C atomic concentration and (c) the corresponding reconstruction for a region of 40 × 40 × 80 nm surrounding the carbon nanotube. (d) Side and top views of CNT planes, where single Fe atoms may be directly coordinated with both C and O atoms. The vacant space is mainly due to the low detection efficiency of the ions. Reproduced from Ref.[137] with permission from Nature Publishing Group. (e) 2D atom map of NiN-graphene shell. The yellow circle represents the selected area of interest in (f) and (g). Scale bar, 10 nm. (f) The 2D projected view of Ni atoms. The green areas represent Ni-rich areas (>50 at %). Away from the Ni sources, there is still a significant number of Ni atoms dispersed in the carbon area. Scale bar, 10 nm. (g) Contour map of Ni concentration with an interval of 2 at %. Reproduced from Ref.[138] with permission from Elsevier.

Identification of SAC active sites

Nanoparticles have facets with crystal orientations that exhibit specific catalytic activity. Intense experimental effort and numerical simulations have been devoted to elucidate the intrinsic catalytic activity of different crystal facets on metal nanoparticles. The supported faceted metal nanoparticles can be divided into five different domains as presented by different colors in **Figure 12a**.[140] The internal metal atoms of the nanoparticles within the metal particle can simply be considered supporting blocks because they do not directly contribute to the catalytic performance. However, these atoms can restructure to reshape the entire particle during the catalytic reactions.[141, 142] The surface or subsurface layers of metal atoms are responsible for the adsorption of reaction species and intermediate product formation during the reactions.[143] The exposed metal atoms at the metal-support interface are often considered active sites for the recombination of adsorbed reactants.[144-146] The interfacial metal atoms, also called buried interfacial atoms, strongly anchor onto the underlying support. Since this buried interfacial region is not perturbed during the catalytic reactions, the strong interaction with the support stabilizes the metal nanoparticles.

In comparison, the catalytic mechanism and associated thermodynamics are profoundly affected when downsizing NP to SACs. Due to their unique structure of isolated metal atoms supported on a matrix, the individual metal atoms of SACs can perform as isolated and independent catalytically active centers.[51] The effects of metal-support interactions on regulating the geometric and electronic structures of central metal species, through which the catalytic properties are further affected, play a central role. For example, compared with nanoparticles, the charge distribution patterns (**Figure 12b**) show a clear electron accumulation (pink area) around the Co atom for Co-Pt SA supported on N-doped carbon but a weak electron accumulation or depletion around Pt atom for Pt-Pt SA on the same

support.[147] This result is attributed to the asymmetric deployment of Pt and Co SAs that polarize surface charges near the active sites.[147] The electrons accumulated on Co sites accelerate the reduction of O_2, which enhances the ORR performance. A similar effect has been predicted from the numerical simulations of Ir SAs supported on TiO_2.[148] Numerical simulations have shown that the catalytic performance of the single-atomic-site Ir on the defective metastable phase of titanium dioxide is attributed to the strength of interactions between active metal sites and reactant molecules. At the Ir SA sites on defected TiO_2, only carbonyl groups interact with the substrate, which results in the significant reduction of adsorption energy compared to that on the Ir nanoparticle. This simple bonding is also expected to facilitate the configuration adjustments of intermediate states during the catalytic reaction. In contrast, for Ir nanoparticles, both furan ring and carbonyl groups interact with the Ir atoms, which results in an overly strong interaction that limits the desorption (**Figure 12c**).[149] In addition, the intermediate states do not effectively adjust their configurations during the reaction process, which impairs the catalytic properties. Theoretical calculations have shown that the coordination not only influences the structure and the electronic characteristics of the SAs, but also the catalytic reaction pathways and the formation of key oxidative species (**Figure 12d**). For example, the increase of Fe-N coordination number facilitates the generation and activation of the crucial intermediate O=Fe=O species, thereby enhancing the activity toward the benzene oxidation reaction (BOR).[150]

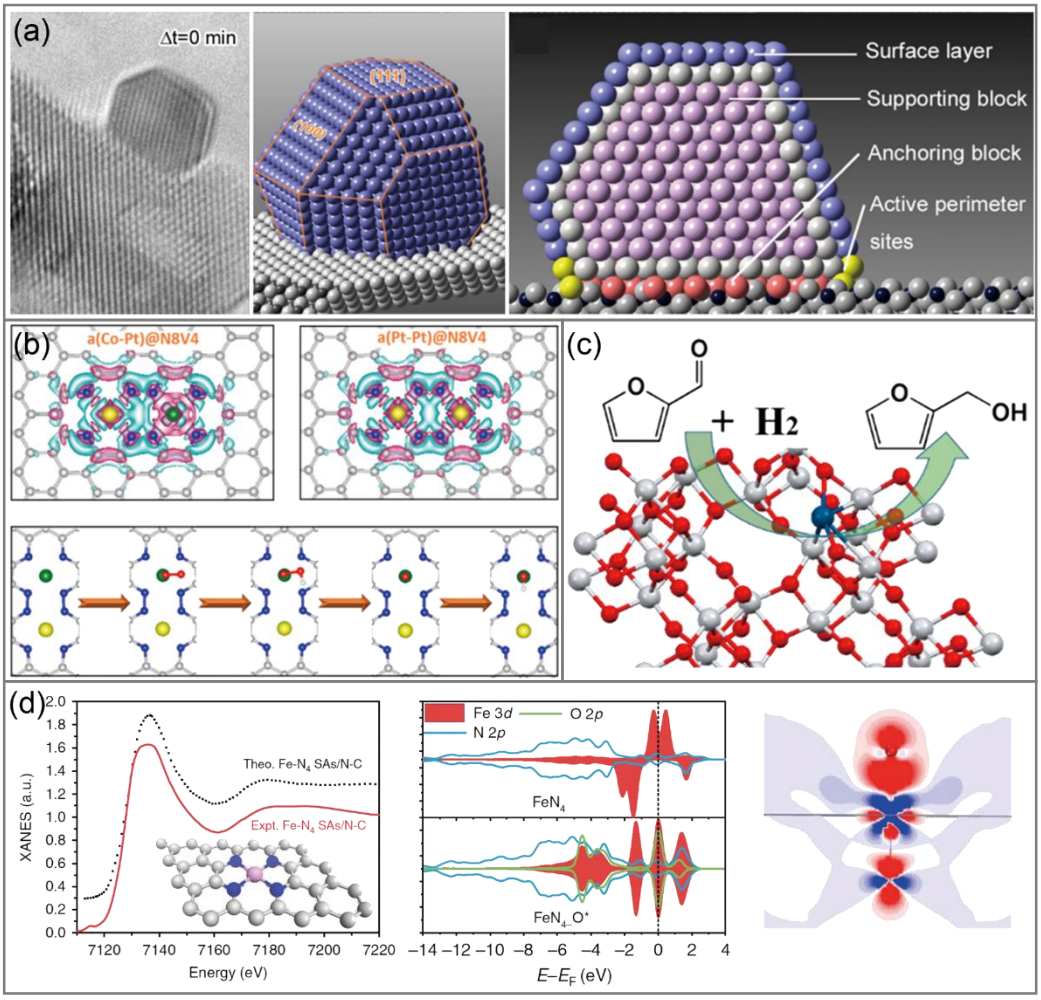

Figure 12 | Identification of the active sites for the SACs. (a) TEM schematic depicting a typical gold nanoparticle atomic scheme of a gold nanoparticle anchoring onto a CeO_2 nanorod, which illustrates the functions of different domains. Reproduced from Ref. [140] with permission from the American Chemical Society. (b) Top view of the charge densities of SA Co on N-doped carbon and SA Pt on the same support. Pink and aqua represent the electron accumulation and depletion areas, respectively. The ORR reaction pathway is illustrated below. Reproduced from Ref. [147] with permission from the American Chemical Society. (c) Experimental results show that the single-atomic-site Ir catalyst supported by the defective metastable phase of titanium dioxide exhibits excellent catalytic performance for the hydrogenation of furfural to furfuryl alcohol. Reproduced from Ref. [149] with permission from the American Chemical Society. (d) XANES spectra, partial density of states (PDOS) and charge density differences analyses of Fe-N_4 SACs. Reproduced from Ref. [150] with permission from the American Chemical Society.

Single atoms as active sites

In the majority of studies on SACs, the single-atom sites are considered the active site. One of the key advantages of single metal atoms as catalytic active sites is the optimization of activity output from the signal atoms. This is particularly important when using precious metals such as Pd, Pt, Ir or Ru. However, it imposes that the noble metal atoms are active and stable on the surface of the support. Zhang and coworkers studied the thermally stable single atom Pt supported on Al_2O_3 for selective hydrogenation and CO oxidation (**Figure 13a**).[86] The catalyst maintains its structural integrity and excellent performance for the selective hydrogenation of 1,3-butadiene even after exposure to a reductive atmosphere at 200 ºC for 24 h. Compared with commercial Pt NP catalysts on Al_2O_3 and control samples, the Pt SAs exhibit significantly enhanced stability and performance towards n-hexane hydroreforming at 550 ºC for 48 h. When tested towards CO oxidation, the Pt single-atom identity is maintained after 60 cycles between 100 and 400 ºC for over one month. The high performance was attributed to the strong anchoring of Pt atoms on the internal surface of mesoporous Al_2O_3 support thanks to the coordination with unsaturated pentahedral Al^{3+} centers.

The choice of support is also an important parameter to optimize the catalytic performance of Pt SACs. For example, there is outstanding activity from Pt SAs embedded in the surface of Ni nanocrystals towards the selective hydrogenation of 3-nitrostyrene (**Figure 13b**).[151] The TOF numbers based on surface Pt atoms of Pt_1/Ni nanocrystals reached ~1800 h^{-1} under 3 atmospheres of H_2 at 40 °C. Importantly, the catalytic activity was significantly enhanced in the case of Ni support compared to active carbon, TiO_2, SiO_2, and zeolite socony mobil-5 (ZSM-5). Mechanistic studies reveal that the remarkable activity of Pt_1/Ni nanocrystals originate from the superior hydrogen supply due to the spontaneous dissociation of H_2 on both Pt and Ni atoms and the facile diffusion of H atoms on Pt_1/Ni

nanocrystals. The ensemble composed of single-atom Pt and nearby Ni atoms in Pt_1/Ni nanocrystals also favors the adsorption of 3-nitrostyrene to activate nitro groups, which accounts for high selectivity towards the production of 3-vinylaniline.

In addition to maximizing the use of noble metal in the catalysis, SACs can change the reaction mechanism compared to traditional metal nanoparticles. Choi and coworkers reported a relatively high loading of atomically dispersed Pt (up to 5.0 wt.%) stabilized on sulfur-doped zeolite-templated carbon with an S content of 17.0 wt.% and a surface area of ~2800 m^2g^{-1}.[152] The electrochemical behavior of such SACs significantly differs from that of cluster-type Pt catalysts. The SA Pt catalysts selectively catalyze the two-electron ORR pathway to produce H_2O_2 instead of the conventional four-electron ORR pathway to produce H_2O. The active sites have been elucidated using DFT calculations as shown in **Figure 13c**. For redox reactions involving multiple electrons, mechanisms typically involve series of proton-coupled electron transfers (PCETs). Theoretical results have suggested that the first PCET on Pt SAs is the potential-determining step for both two- and four-electron processes. In the case of the two-electron pathway, H_2O_2 is generated during the second PCET and subsequently desorbs using additional water molecules from the electrolyte. The Pt SAs return to their initial state, where Pt is complexed with two thiolates and two water molecules. The four-electron pathway, which leads to the formation of H_2O via the O-O bond dissociation, is less energy favorable.

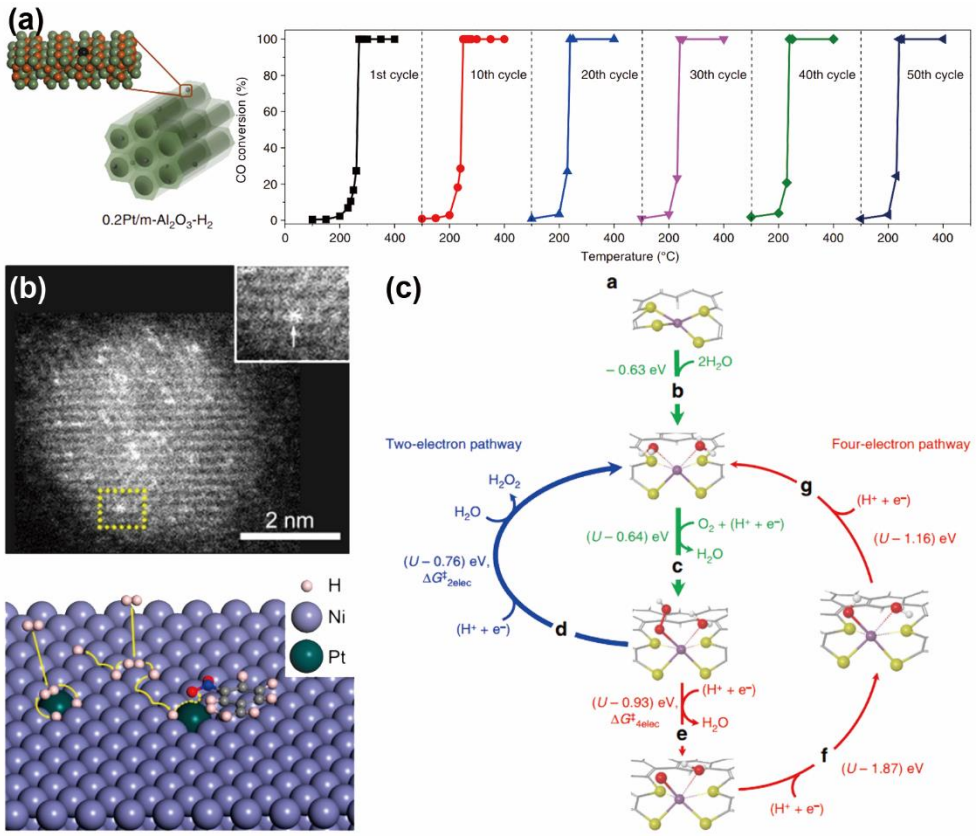

Figure 13 | Single atom acting as catalytic active sites. (a) Scheme of the single-atom catalyst 0.2Pt/m-Al_2O_3-H_2 and long-term thermal stability with conversion of CO from 100 to 400 °C with 1st 50th cycles. Reproduced from Ref. [86] with permission from Nature Publishing Group. (b) HAADF-STEM image of an individual 1.0 wt.% Pt_1/Ni nanocrystal and schematic illustration of the H_2 dissociation and H diffusion on Pt_1/Ni(111). Reproduced from Ref. [151] with permission from the American Chemical Society. (c) Proposed ORR mechanism on the atomically dispersed Pt catalyst. Reproduced from Ref. [152] with permission from Nature Publishing Group.

Single atoms as cocatalysts

While most studies on SACs consist of individual atoms as catalytically active sites, few examples have been reported of metal SAs acting as cocatalysts to improve the catalytic performance by introducing local perturbation in the electronic structure of the support. Therefore, a careful choice of the supports to tune the interactions with the SAs is desirable for efficient and selective electrocatalysts by increasing the number and reactivity of active sites. This approach requires a balance between

several conflicting factors, such as sufficient electrical conductivity, suitable energy band structure and abundant defects. For example, the preparation of metal single atom (Pt, Co, Ni) on MoS_2 can activate the in-plane S atoms, which are generally considered inert for HER.[68] HAADF-STEM and XAFS characterization reveals that single Pt atoms can successfully replace some Mo atoms in MoS_2. DFT calculations predict that the single metal atoms modify the adsorption mode of hydrogen atoms in neighboring S sites thus improving the thermodynamics of the reaction (**Figure 14a**).

With regard to the increase in reactivity at the active sites, tuning the coordination environment of metal single atoms and generating synergy effects between the single atoms and the support appears promising. Gold is not an optimized catalyst for the oxygen evolution reaction (OER), but Au SAs have been found to modify the adsorption energies of OER intermediates on active sites, which leads to superior OER activity. Single-atom Au supported on NiFe layered double hydroxides (LDH) is a highly efficient and robust OER electrocatalyst (**Figure 14b**).[153] To address the reaction mechanism, the transformation of surface charge of SACs with adsorbed O* was investigated. The activity originates from the Fe atoms in NiFe oxyhydroxide support and the Au atoms are predicted to sit on top of O atoms of LDH with the orientation of Au-O bond parallel to the c-axis. In this configuration, the five degenerated *d* orbitals of Au are spatially redistributed, which induces an increase in charge density around the ring region of Au parallel to the surface direction. The integrated charge density difference yields a net Au-to-LDH charge redistribution of 0.32 electron, which transfers to the surrounding O, Ni and Fe atoms. Ultimately, the electron transfer between single atom Au and the LDH support facilitates the adsorption of OH^- and modifies the adsorption energies of O* and OOH* intermediates, which results in low overpotential in the rate-limiting step from O* to OOH*. In some cases, the catalytic active site is comprised of a single metal atom and its neighboring

atoms. Considering Pt SAs supported on g-C_3N_4 as a photocatalytic assembly towards the H_2 evolution, the coordination environment of the transition metal Pt is responsible for the H_2 evolution activity (**Figure 14c**).[154] However, the g-C_3N_4 supports participate in the reaction via strong interactions with the N groups, which stabilize the metal single metal atoms and tailor the catalytic properties by locally changing the electronic structure of the metal single atom and the support.[155]

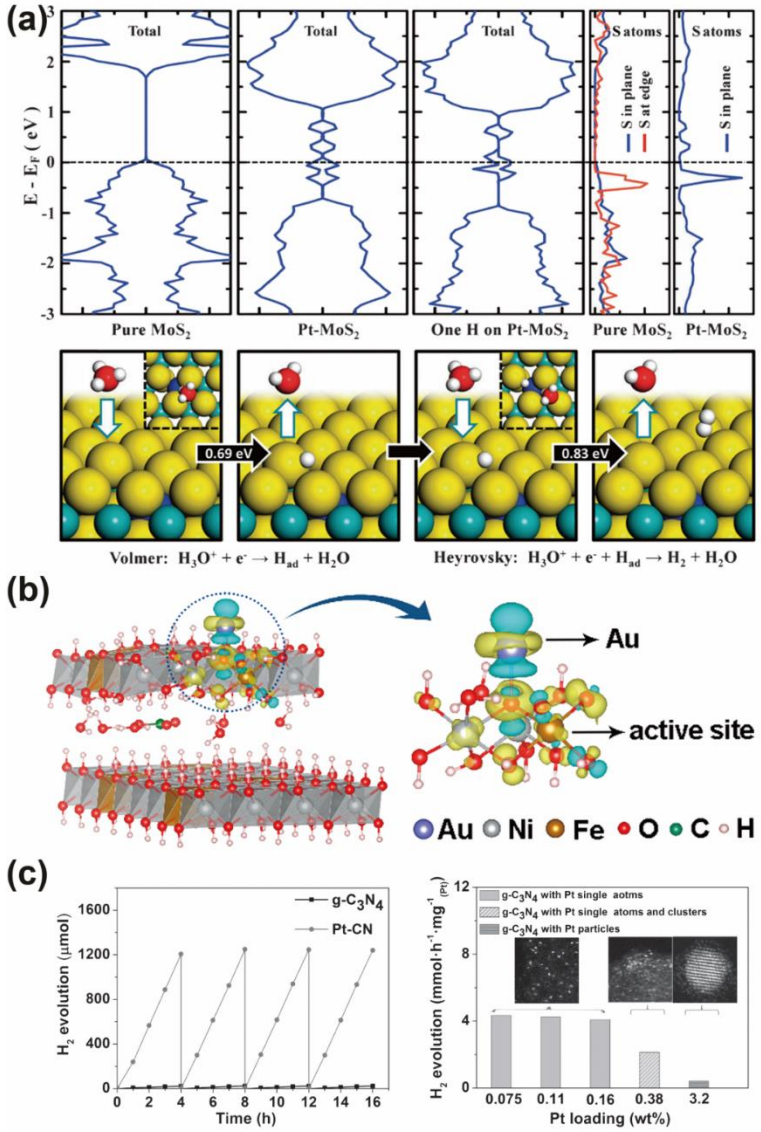

Figure 14 | Single atom acting as a cocatalyst. (a) Total DOS for the pure MoS_2, Pt-MoS_2, one H absorbed on Pt-MoS_2, and projected DOS of the in-plane and edge S atoms from pure MoS_2 and Pt-MoS_2, respectively. The position of the Fermi level is shown in dashed lines; HER process on a Pt-MoS_2 catalyst. The top views are shown in the insets. The reaction barriers are shown in the black arrows. The green, yellow, blue, red and white balls represent Mo, S, Pt, O and H atoms,

respectively. Reproduced from Ref. [68] with permission from Royal Society of Chemistry. (b) Differential charge densities of NiFe LDH with and without Au atom when one O atom is adsorbed on the Fe site. The yellow and blue contours represent the electron accumulation and depletion, respectively. Reproduced from Ref. [153] with permission from the American Chemical Society. (c) Photocatalytic H_2 evolution generation activity of g-C_3N_4 and Pt-CN with different Pt contents and loading amounts normalized per Pt atom. Reproduced from Ref. [154] with permission from Wiley.

Conclusions and Outlook

Downsizing the metal particles from nanometer to sub-nanometer scale and ultimately to single atoms has proven to be an efficient strategy to obtain attractive catalytic properties. Rapid progress of the fundamental understanding of interactions between the metal atoms and the support have led to a paradigm shift in the field of conventional metal-supported catalysis. The strong metal single atoms-support interactions stabilize the atomically dispersed metal sites and provide an additional knob to tune the electronic structure of the single-atom metal and its coordination environment to optimize the catalytic performance. Therefore, the synthesis routes and characterization techniques are critical. In this review, we analyzed the recent progress in the field by summarizing different interactions between the metal single atoms and the support. The techniques to characterize the metal-support interactions and identify the active sites are presented. We reviewed the current understanding of the interactions between the metal single atoms and the support to design and prepare highly stable SACs. Although single-atom catalysis has achieved many encouraging advances, many challenges remain to be addressed regarding the (i) synthesis, (ii) optimization of catalytic performance, (iii) elucidation of the interactions between single atoms and support and (iv) combination of theoretical and experimental methods to better describe the reaction mechanisms. As an outlook for the field, we highlight a few key remaining challenges for SACs.

(i) *Improving loading of SACs.* Two of the main bottlenecks of single-atom catalysis are the low loading of SAs and lack of scalable synthesis methods. The reported SACs are also limited to only a

few metals. For practical applications, high performance will require a high density of single metal atoms for abundant active sites; therefore, novel synthetic routes that are simple, scalable and economically viable must be developed.

(ii) Optimizing the activity of SACs. The development of molecular bimetallic or trimetallic centers may broaden the applications of atomic catalysts *via* the creation of synergistic effects.[156] While hundreds of papers have reported on SACs, only a few have reported dinuclear and multinuclear species without organic ligands as active sites.[98] In this regard, there is a clear gap between SACs and the well-studied nanoparticle catalysts. An atom-by-atom approach to synthesize active sites ranging from single atoms to atomically precise metal clusters on the same support is highly desirable. Thus, the concept of single-atom catalyst has been recently extended to single-cluster catalyst (SCC), but the nuclearity effect on heterogeneous catalysis has not been systematically studied, understood, and rationalized.[157] We expect that research in this direction to control the coordination environment of metal atoms holds great promise for optimizing and improving the catalytic properties of SACs.

(iii) Understanding the interactions between the single atoms and the support. In atomically dispersed metal catalysis, all catalytic metal atoms directly interact and coordinate with the supports. In other words, the supports serve as the ligands to metal centers as is the situation in homogeneous organometallic catalysts. Therefore, compared with the supported metal nanocatalysts, the nature of the support plays a more important role in determining the overall catalysis mechanisms and performance of atomically dispersed metal catalysts. The local coordination environments of metal in different atomically dispersed catalysts can be completely different. Thus, it is not surprising that the same metal atoms dispersed on different supports exhibit different catalytic properties and sometimes

even contradictory performance. The investigation of the vicinity of metal atoms (e.g., the binding elements, metal coordination structures, and redox properties of adjacent metals) is crucial to understanding their catalytic mechanisms.[158]

(iv) *Combining numerical and experimental methods.* Any progress in the field of SACs will rely on the necessary combination between experimental work and numerical simulations to tackle the remaining fundamental questions regarding the structure-activity relationship and catalytic mechanism at the atomic scale. However, key challenge remains in the poor matching between theoretical and experimental results. To achieve a more comprehensive understanding of the nature of single-atom catalysis, the dynamic behaviors and possible structural change of catalysts during catalysis should be considered in terms of theoretical simulations. *Operando* characterizations such as *in situ* electron microscopy and XAFS are crucially required to provide a better picture of the evolution of the single-atom active site during the reaction.

Acknowledgments

D.V. and K.Q. acknowledge the financial support from the European Research Council (ERC) under the European Union's Horizon 2020 Research and Innovation Program (grant agreement No 804320). We express our sincere thanks to Yang Zhang, Huali Wu and Wensen Wang for fruitful discussions and assistance.

References

[1] H. Li, et al., Nat. Nanotechnol., 13 (2018) 411-417.
[2] P. Peng, et al., Sci. Adv., 5 (2019) eaaw2322.
[3] A. Wang, et al., Nat. Rev. Chem., 2 (2018) 65-81.

[4] S. Tauster, et al., J. Am. Chem. Soc., 100 (1978) 170-175.
[5] H. Tang, et al., J. Am. Chem. Soc., 138 (2016) 56-59.
[6] J. Dong, et al., J. Am. Chem. Soc., 140 (2018) 13808-13816.
[7] W.E. Kaden, et al., Science, 326 (2009) 826-829.
[8] P. Hu, et al., Angew. Chem. Int. Ed., 53 (2014) 3418-3421.
[9] X. Yang, et al., Acc. Chem. Res. , 46 (2013) 1740-1748.
[10] Y. Yao, et al., Nat. Nanotechnol., 14 (2019) 851-857.
[11] J. Liu, ACS Catal., 7 (2016) 34-59.
[12] S. Mitchell, et al., Angew. Chem. Int. Ed., 57 (2018) 15316-15329.
[13] H. Zhang, et al., Adv. Energy Mater., 8 (2018) 1701343.
[14] X. Cui, et al., Nat. Catal., 1 (2018) 385.
[15] J. Zhang, et al., Small Methods, 3 (2019) 1800481.
[16] P. Li, et al., Mater. Today, 35 (2020) 78-86.
[17] M.T. Darby, et al., ACS Catal., 8 (2018) 5038-5050.
[18] F.R. Lucci, et al., Nat. Commun., 6 (2015) 8550.
[19] M.D. Marcinkowski, et al., Nat. Chem., 10 (2018) 325.
[20] T. Yamada, et al., J. Am. Chem. Soc., 140 (2018) 3838-3841.
[21] G.X. Pei, et al., ACS Catal., 5 (2015) 3717-3725.
[22] L. Zhang, et al., Natl. Sci. Rev., 5 (2018) 653-672.
[23] J. Liu, et al., ACS Catal., 9 (2019) 8757-8765.
[24] G. Kyriakou, et al., Science, 335 (2012) 1209-1212.
[25] M.T. Greiner, et al., Nat. Chem., 10 (2018) 1008.
[26] L. Cao, et al., Nat. Catal., 2 (2019) 134-141.
[27] Y. Xiong, et al., Nat. Nanotechnol., 15 (2020) 390-397.
[28] T. Zheng, et al., Joule, 3 (2019) 265-278.
[29] F. Yang, et al., Angew. Chem. Int. Ed., 57 (2018) 12303-12307.
[30] S. Liu, et al., Angew. Chem. Int. Ed., 58 (2019) 2-8.
[31] J. Zhao, et al., Proc. Natl. Acad. Sci., 111 (2014) 15641-15646.
[32] H. Yan, et al., J. Am. Chem. Soc., 137 (2015) 10484-10487.
[33] Y. Hou, et al., Nat. Commun., 10 (2019) 1392.
[34] Y. Pan, et al., J. Am. Chem. Soc., 140 (2018) 4218-4221.
[35] Y. Xue, et al., Nat. Commun., 9 (2018) 1460.
[36] Z.Z. Lin, Carbon, 108 (2016) 343-350.
[37] R. Shen, et al., Chem, 5 (2019) 2099-2110.
[38] H. Tao, et al., Chem, 5 (2019) 204-214.
[39] J. Zhang, et al., Nat. Catal., 1 (2018) 985.
[40] H. Xiong, et al., Angew. Chem. Int. Ed., 56 (2017) 8986-8991.
[41] C.K. Poh, et al., J. Phys. Chem. C, 118 (2014) 13525-13538.
[42] L. Lin, et al., Nature, 544 (2017) 80.
[43] S. Yang, et al., ACS Catal., 7 (2017) 1301-1307.
[44] D. Zhao, et al., J. Am. Chem. Soc., 141 (2019) 4086-4093.
[45] D.A. Kuznetsov, et al., J. Am. Chem. Soc., 141 (2019) 17809-17816.
[46] Z. Chen, et al., Adv. Mater., 32 (2020) 1906437.
[47] X. Dai, et al., ACS Appl. Mater. Interface, 7 (2015) 27242-27253.

[48] K. Qi, et al., Nat. Common., 10 (2019) 5231.
[49] Y.C. Lin, et al., Nat. Nanotechnol., 9 (2014) 391.
[50] F.R. Lucci, et al., Nat. Common., 6 (2015) 8550.
[51] M. Li, et al., Nat. Catal., 2 (2019) 495-503.
[52] X.P. Yin, et al., Angew. Chem. Int. Ed., 57 (2018) 9382-9386.
[53] J. Liu, et al., J. Am. Chem. Soc., 138 (2016) 6396-6399.
[54] Q. Li, et al., Adv. Mater., 30 (2018) 1800588.
[55] P. Chen, et al., Angew. Chem. Int. Ed., 56 (2017) 610-614.
[56] C. Zhao, et al., Joule, 3 (2019) 584-594.
[57] Y. Lin, et al., Adv. Mater., 31 (2019) 1808193.
[58] J. Gu, et al., Science, 364 (2019) 1091-1094.
[59] X.X. Wang, et al., Adv. Mater., 30 (2018) 1706758.
[60] W. Zang, et al., ACS Catal., 8 (2018) 8961-8969.
[61] X. He, et al., Nat. Common., 10 (2019) 3663.
[62] H.T. Chung, et al., Science, 357 (2017) 479-484.
[63] Y. Han, et al., J. Am. Chem. Soc., 139 (2017) 17269-17272.
[64] L. Han, et al., Angew. Chem. Int. Ed., 131 (2019) 2343-2347.
[65] Y. Zhao, et al., Adv. Energy Mater., 8 (2018) 1702524.
[66] H. Yan, et al., Nat. Commun., 9 (2018) 3197.
[67] G. Liu, et al., Nat. Chem., 9 (2017) 810-816.
[68] J. Deng, et al., Energy Environ. Sci., 8 (2015) 1594-1601.
[69] Y. Wang, et al., Nano-Micro Lett., 11 (2019) 102.
[70] S. Yang, et al., Angew. Chem. Int. Ed., 55 (2016) 2058-2062.
[71] B. Qiao, et al., Nat. Chem., 3 (2011) 634-641.
[72] H. Wei, et al., Nat. Common., 5 (2014) 5634.
[73] J. Lin, et al., J. Am. Chem. Soc., 135 (2013) 15314-15317.
[74] R. Lang, et al., Angew. Chem. Int. Ed., 55 (2016) 16054-16058.
[75] Y. Zhao, et al., J. Am. Chem. Soc., 141 (2019) 10590-10594.
[76] M.M. Millet, et al., J. Am. Chem. Soc., 141 (2019) 2451-2461.
[77] Y. Chen, et al., Joule, 2 (2018) 1242-1264.
[78] A. Corma, et al., Nat. Chem., 5 (2013) 775.
[79] R. Qin, et al., Small Methods, 2 (2018) 1700286.
[80] S. Ding, et al., Joule, 3 (2019) 2897-2929.
[81] S. Abbet, et al., J. Am. Chem. Soc., 122 (2000) 3453-3457.
[82] L. Zhang, et al., Energy Environ. Sci., 12 (2019) 492-517.
[83] S. Liang, et al., ChemCatChem, 7 (2015) 2559-2567.
[84] C. Zhu, et al., Angew. Chem. Int. Ed., 56 (2017) 13944-13960.
[85] M. Yang, et al., J. Am. Chem. Soc., 135 (2013) 3768-3771.
[86] Z. Zhang, et al., Nat. Commun., 8 (2017) 16100.
[87] P. Liu, et al., Science, 352 (2016) 797-800.
[88] H. Wei, et al., Nat. Common., 8 (2017) 1490.
[89] Q. Wang, et al., Energy Environ. Sci., 12 (2019) 1730-1750.
[90] Y. Zhang, et al., Small Methods, 3 (2018) 1800406.
[91] Z. Geng, et al., Adv. Mater., 30 (2018) 1803498.

[92] R. Lang, et al., Nat. Commun., 10 (2019) 234.
[93] J. Wan, et al., Adv. Mater., 30 (2018) 1705369.
[94] S. Ida, et al., J. Am. Chem. Soc., 137 (2014) 239-244.
[95] J. Zhang, et al., Nat. Common., 9 (2018) 1002.
[96] H. Li, et al., ACS Nano, 11 (2017) 3392-3403.
[97] L. Li, et al., ACS Nano, 13 (2019) 6824-6834.
[98] H. Yan, et al., Nat. Common., 8 (2017) 1070.
[99] J. Yang, et al., ACS Nano, 13 (2019) 9958-9964.
[100] H.J. Qiu, et al., Angew. Chem. Int. Ed., 54 (2015) 14031-14035.
[101] X. Zhang, et al., Nat. Common., 4 (2013) 1924.
[102] L. Zhang, et al., Chem, 4 (2018) 285-297.
[103] C. Zhao, et al., J. Am. Chem. Soc., 139 (2017) 8078-8081.
[104] X. Fang, et al., Adv. Mater., 30 (2018) 1705112.
[105] A. Han, et al., Small Methods, 3 (2019) 1800471.
[106] L. Jiao, H.L. Jiang, Chem, 5 (2019) 786-804.
[107] J. Wang, et al., J. Am. Chem. Soc., 139 (2017) 17281-17284.
[108] X. Wang, et al., J. Am. Chem. Soc., 139 (2017) 9419-9422.
[109] S. Wei, et al., Nat. Nanotechnol., 13 (2018) 856.
[110] B. Zhang, et al., Adv. Sci., 6 (2019) 1901787.
[111] H. Xu, et al., Nat. Catal., 1 (2018) 339.
[112] Y. Ren, et al., Nat. Common., 10 (2019) 4500.
[113] X. Wang, et al., Angew. Chem. Int. Ed., 57 (2018) 1944-1948.
[114] H.L. Fei, et al., Nat. Catal., 1 (2018) 63-72.
[115] Y. Qu, et al., Nat. Catal., 1 (2018) 781.
[116] Z. Pu, et al., Nano-Micro Lett., 12 (2020) 1-29.
[117] Y. Zhao, et al., Angew. Chem. Int. Ed., 58 (2019) 12252-12257.
[118] X. Mou, et al., Radiat. Phys. Chem., (2019) DIO: 10.1016/j.radphyschem.2019.1003.1034.
[119] L. Cao, et al., Nat. Common., 10 (2019) 1.
[120] D. Koziej, Chem. Mater., 28 (2016) 2478-2490.
[121] Y. Pan, et al., Angew. Chem. Int. Ed., 57 (2018) 8614-8618.
[122] M. Liu, et al., Energy Environ. Sci., 12 (2019) 2890-2923.
[123] Q. He, et al., Adv. Funct. Mater., (2020) 2000407.
[124] L. Yang, et al., Nat. Energy, 50 (2018) 691-698.
[125] H.B. Yang, et al., Nat. Energy, 3 (2018) 140-147.
[126] R. Sarangi, et al., Biochemistry, 48 (2009) 3146-3156.
[127] L. Mogg, et al., Nat. Nanotechnol., (2019) 1-5.
[128] H.L. Jiang, et al., Angew. Chem. Int. Ed., 59 (2019) 2705-2709.
[129] A. Zitolo, et al., Nat. Mater., 14 (2015) 937.
[130] W. Liu, et al., Chem. Sci., 7 (2016) 5758-5764.
[131] T.H.M. Lau, et al., Chem. Sci., 9 (2018) 4769-4776.
[132] J. Mao, et al., Nat. Common., 9 (2018) 4958.
[133] G. Liu, et al., Nat. Chem., 9 (2017) 810.
[134] N. Cheng, et al., Electrochem. Energ. Rev., 2 (2019) 539-573.
[135] F.R. Lucci, et al., J. Phys. Chem. Lett., 7 (2016) 480-485.

[136] D. Zhao, et al., Chem. Soc. Rev., 49 (2020) 2215-2264.
[137] K. Jiang, et al., Nat. Common., 10 (2019) 3997.
[138] K. Jiang, et al., Chem, 3 (2017) 950-960.
[139] H. Fei, et al., Chem. Soc. Rev., 48 (2019) 5207-5241.
[140] N. Ta, et al., J. Am. Chem. Soc., 134 (2012) 20585-20588.
[141] K. Qi, et al., Nanoscale, 8 (2016) 1698-1703.
[142] Y. Yao, et al., Nat. Catal., 2 (2019) 304-313.
[143] S. Kattel, et al., J. Am. Chem. Soc., 139 (2017) 9739-9754.
[144] K. Ding, et al., Science, 350 (2015) 189-192.
[145] N.R. Sahraie, et al., Nat. Common., 6 (2015) 8618.
[146] K. Qi, et al., J. Mater. Chem. A, 4 (2016) 4025-4031.
[147] L. Zhang, et al., J. Am. Chem. Soc., 140 (2018) 10757-10763.
[148] J.K. Nørskov, et al., Nat. Chem., 1 (2009) 37.
[149] S. Tian, et al., ACS Catal., 9 (2019) 5223-5230.
[150] Y. Pan, et al., Nat. Common., 10 (2019) 4290.
[151] Y. Peng, et al., Nano Lett., 18 (2018) 3785-3791.
[152] C.H. Choi, et al., Nat. Commun., 7 (2016) 10922.
[153] J. Zhang, et al., J. Am. Chem. Soc., 140 (2018) 3876-3879.
[154] X. Li, et al., Adv. Mater., 28 (2016) 2427-2431.
[155] Z. Chen, et al., Adv. Mater., 30 (2018) 1704720.
[156] J. Wang, et al., Sci. Adv., 4 (2018) eaap7970.
[157] X. Ma, et al., J. Am. Chem. Soc., 140 (2017) 46-49.
[158] E. Fako, et al., Catal. Sci. Technol., 7 (2017) 4285-4293.